Document title	Experimental Investigation of Ti–Al–Si Phase Equilibria at 800–1200 °C
Authors	Zahra Kahrobaee, Martin Palm
Issue date	August 28, 2022
Journal	Journal of Alloys and Compounds
DOI	10.1016/j.jallcom.2022.166223
Acknowledgment	This project has received funding from the Clean Sky 2 Joint Undertaking under the European Union's Horizon 2020 research and innovation programme under grant agreement No 820647.
Disclaimer	The content of this article reflects only the author's view. The Clean Sky Joint Undertaking is not responsible for any use that may be made of the information it contains.

ADVANCE

Journal of Alloys and Compounds 924 (2022) 166223

Contents lists available at ScienceDirect

Journal of Alloys and Compounds

journal homepage: www.elsevier.com/locate/jalcom

Experimental investigation of Ti–Al–Si phase equilibria at 800–1200 °C

Zahra Kahrobaee*, Martin Palm

Max-Planck-Institut für Eisenforschung GmbH (MPIE), Max-Planck-Straße 1, 40237 Düsseldorf, Germany

ARTICLE INFO

Article history:
Received 11 March 2022
Received in revised form 5 July 2022
Accepted 6 July 2022
Available online 8 July 2022

Keywords:
Phase diagram
Phase transitions
Microstructure
Crystal structures

ABSTRACT

Five partial isothermal sections of the Ti–Al–Si system up to 70 at% Al and 40 at% Si have been determined experimentally between 800 and 1200 °C. Seven alloys were heat-treated for 24–1504 h and characterized utilizing scanning electron microscopy, electron probe microanalysis, X-ray diffraction, and differential thermal analysis. No ternary phase was found and αTi, βTi, Ti_3Al, TiAl, TiAl(1d-APS), $TiAl_2$, $TiAl_3$ are in equilibrium with Ti_5Si_3. A partial vertical section at 9 at% Si shows that all determined data are consistent with each other.

1. Introduction

TiAl-based alloys are by now an established class of high-temperature materials. Low-pressure turbine blades manufactured from TiAl-based alloys are used in GEnx™ commercial aircraft engines since more than a decade. The application of TiAl-based alloys in aero engines successfully decreased the amount of fuel consumption, thereby substantially reducing gas emissions [1]. This success is due to the low density of TiAl-based alloys compared to Ni-based superalloys, which they have replaced. TiAl-based alloys show similar specific strength to Ni-based superalloys, which enables them to replace superalloys at application temperatures between 600–800 °C [2]. In order to enable even higher application temperatures, their creep and high-temperature oxidation resistance have to be improved which can be achieved through tailoring the microstructure and alloying [2,3].

The oxide scale which forms on TiAl-base alloys is a multilayer that consists of TiO_2 and Al_2O_3 [3]. TiO_2 is porous and therefore cannot inhibit the metal surface from further oxidation. Alloying with Si can improve the oxidation resistance through different mechanisms. Si refines TiO_2 particles, which results in the formation of a more compact oxide scale [3]. Si also facilitates Al diffusion in the scale and hinders the outward diffusion of Ti^{4+}, thereby prohibiting further formation of TiO_2. About 10 at% Si are sufficient for the preferential formation of Al_2O_3, which forms a protective oxide scale [4]. Even higher Si contents promote the formation of SiO_2 in the oxide scale. It is assumed that the lower diffusion coefficient of oxygen in SiO_2 compared to TiO_2 and the formation of a TiN layer between the base material and the oxide scale lead to a decrease in the oxidation rate [5,6].

Moreover, Si is known to be beneficial in improving the creep resistance through the formation of fine-scaled Ti_5Si_3 precipitates [7,8]. Adding about 0.3 at% Si can lead to the formation of Ti_5Si_3 at the Ti_3Al/TiAl lamellar interface. Ti_5Si_3 particles substantially increase the creep resistance by hindering the movement of dislocations. For an alloy with about 0.6 at% Si, a ten times higher creep rate has been achieved compared to its Si-free counterpart [7,8]. On the other hand, a small excess amount of Si deteriorates the microstructure, thus reducing fracture toughness and creep resistance [7]. Though there is an apparent discrepancy between the optimum Si contents for improving creep and oxidation resistance at the same time only by Si, it was observed recently that of two alloys produced by powder metallurgy and containing 21 and 28 at% Si, the alloy with the higher amount of Si showed a lamellar structure coupled with larger silicides, which yielded a better toughness [9].

For the development of new TiAl-based alloys with improved properties, the knowledge of the constituent phases and phase transformations in dependence on temperature and composition is crucial. As commercial alloys usually comprise a large number of elements, CALPHAD (CALculation of PHAse Diagram) modeling is usually employed to envisage phase equilibria of higher-order systems [10]. The results can be used to predict e.g. compositions, which yield a specific volume fraction of Ti_5Si_3 for improving the creep resistance, or windows for thermomechanical processing or heat treatments to generate individual microstructures. Since CALPHAD relies on the extrapolation of thermodynamic data from

* Corresponding author.
E-mail addresses: z.kahrobaee@mpie.de (Z. Kahrobaee), palm@mpie.de (M. Palm).

https://doi.org/10.1016/j.jallcom.2022.166223
0925-8388/

binary and ternary systems, the reliability of the results crucially depends on the underlying database, i.e. the availability and quality of experimental results from the constituent binary and ternary systems [10].

1.1. Literature review

The Ti–Al–Si system has been thoroughly assessed within the MSI Ternary Phase Diagram Evaluation scheme [11,12], considering references for the ternary system up to 2002 and has been reviewed by Raghavan [13,14], covering references up to 2008. In the following, a summary of investigations focusing on phase equilibria in the Ti-rich part of the system is given.

Bulanova et al. [15,16] established three partial isothermal sections at 1250, 1270 and 1300 °C, a liquidus and solidus diagram for the complete Ti—Al—Si system, four vertical sections at 5 and 10 at% Si, 50 at% Ti, 40 at% Al and a reaction scheme using metallography, differential thermal analysis (DTA), X-ray diffraction (XRD), and electron probe microanalysis (EPMA) of annealed and as-cast alloys. Based on XRD of samples annealed for 6–12 h, Schob et al. [17] established a complete isothermal section at 1200 °C. Turner and Crossley [18,19] established partial isothermal sections of the Ti corner at 600, 800, 900, 1000, 1100, and 1200 °C and two partial vertical sections for 2 and 6 wt% Al from light optical microscopy. Li et al. [20,21] established a partial vertical section for 0.3 at% Si from EPMA measurements showing the Ti_3Al/TiAl and αTi/TiAl phase boundaries between 1000 and 1250 °C. Azevedo and Flower [22–24] carried out a comprehensive study of the Ti-rich part of the system employing XRD, scanning and transmission electron microscopy (SEM, TEM), both combined with energy-dispersive spectroscopy (EDS). They established partial isothermal sections at 700, 800, 900, and 1100 °C [22] and calculated partial isothermal sections for the temperature range 700–1200 °C [23,24]. From XRD and EPMA results of a single sample and data from literature Viala et al. [25] created a simplified isothermal section at 1000 °C. Gupta [26] studied the phase equilibria in the temperature range 700–1000 °C employing ternary diffusion couples between pure titanium and a eutectic Al–Si alloy. Compositions of the phases were established through EPMA. An isothermal section at 1000 °C was constructed and phase equilibria at the remaining temperatures were discussed. Liu et al. [27] established an isothermal section at 1000 °C and a partial isothermal section at 900 °C focusing on the Al-rich side utilizing EDS measurements of heat-treated alloys. Additionally, they determined the liquidus surface by performing DTA up to 1500 °C. A complete isothermal section at “about 700 °C” was determined employing metallography and XRD of annealed alloys by Raman & Schubert [28]. Apparently, the term “about” was chosen because the authors realized that annealing times of 48 – 120 h may have been too short to attain equilibrium in all investigated alloys. Based on the work of Raman & Schubert [28], Gröbner et al. [29] calculated the isothermal section at 700 °C. More recently, a complete isothermal section at 700 °C has been established by XRD and EDS on alloys that were homogenized at 1100 °C for 40 h and then equilibrated at 700 °C for 1080 h [30]. Based on a number of experimental data from Al—Si-rich alloys, complete isothermal sections at 550, 585, 590, 650, 727 and 900 °C were calculated by Li et al. [31]. A complete isothermal section at 550 °C was established by Wang et al. [32] using SEM, EDS and XRD on annealed alloys. Finally, a complete isothermal section at 20 °C was presented by Kamei et al. [33] from microstructures and XRD of as-cast alloys.

Despite all the investigations mentioned above, data on phase equilibria are at least partially controversial. For instance for the solid solubility of Si in TiAl at 1000 °C, reported data vary between 0.1 [20] and about 3 at% [26,27] and data for the solid solubility of Al in Ti_5Si_3 vary between 2 [22] and 11 at% [27]. It is noted that in alloys produced through powder metallurgy even much higher Al contents up to more than 20 at% Al have been observed in Ti_5Si_3 [34–36], but it is assumed that these compositions are metastable [36]. However, the knowledge of the precise solid solubilities of both phases in dependence on temperature is essential for the design of more creep resistant TiAl-based alloys, because this information yields the volume fraction of Ti_5Si_3 at a certain temperature for a given composition.

In order to improve these and other thermodynamic data, which are relevant for the development of TiAl alloys with improved properties, several Ti–Al–X(–Y) systems are investigated within the large-scale European project ADVANCE to set up the next generation of advanced CALPHAD databases for Ti–Al alloys [37]. As a part of this project, phase equilibria between the Ti–Al phases and Ti_5Si_3 between 800 and 1200 °C, the temperature range where the alloys are processed and maybe applied, were experimentally investigated.

2. Materials and methods

From elements of high purity (Ti: 99.995%; Al: 99.999%; Si: 99.99%) seven alloys were prepared by crucible-free levitation melting (Fives Celes) [38] or advanced arc melting (PINK GmbH Vakuumtechnik). These techniques have been chosen in view that phase equilibria in Ti–Al(–X) are crucially affected by impurities, especially oxygen [39]. In contrast to conventional arc melters, the advanced device is equipped with a manipulator, which allows overturning the solidified material without opening the device, thereby maintaining a good vacuum during the whole melting process. Moreover, the alloys do not solidify on the cold copper hearth but are cast into a Cu mold. Advanced arc melting has been used for alloys S2 and S3 (Table 1), which could not be fully molten by levitation melting. Rods of 15–18 mm in diameter and 150 mm in length were produced by both methods by casting into cold copper molds. Wet-chemical analysis of slices taken from the top and bottom of the alloys showed that the alloys were homogeneous within standard error. Alloys produced by crucible-free levitation melting showed an average amount of about 100 wt% ppm O, while those produced by advanced arc melting contained 260 and 430 wt% ppm oxygen. Overall compositions of the alloys and impurity contents have been determined by wet-chemical analysis, employing inert gas fusion (NCS Fusion Master ONH) for oxygen and nitrogen, combustion gas analysis (NCS Combustion Master CS) for carbon, and inductively coupled plasma optical emission spectroscopy (PerkinElmer Optima 8300 ICP-OES) for all other elements. The results are summarized in Table 1.

For heat-treatments at 800–1100 °C, slices of the alloys were encapsulated in high-purity quartz capsules back-filled with Ar and using Ti as a getter. Heat-treatments at 1200 °C, where quartz capsules are not any longer gas-tight [40], were performed under flowing dry Ar using a double-crucible technique [38,41]. After annealing at 1200 °C/24 h, 1100 °C/165–200 h, and 800–1000 °C/1000–1504 h, all samples were quenched to room temperature.

Microstructures were inspected using a SEM (Zeiss LEO 1550 VP). Phases were identified by XRD (Bruker Advance D8) using powders with a particle size of < 90 µm. XRD measurements were performed

Table 1
Wet-chemical analyses of the as-cast alloys.

Alloy	Ti (at%)	Al (at%)	Si (at%)	O (wt. ppm)	N (wt. ppm)	C (wt. ppm)
S1	37.5	55.0	7.5	110	< 50	92
S2	43.5	47.4	9.1	260	< 50	100
S3	50.7	40.4	8.9	430	< 50	120
S4	60.2	32.7	7.1	85	< 50	75
S5	71.0	20.4	8.6	70	< 50	97
S6	75.8	14.7	9.5	105	< 50	110
S7	80.7	9.7	9.6	130	< 50	129

Table 2
Crystallographic data of solid phases.

Phase	Pearson Symbol, Space Group, Prototype	Lattice Constants (nm)	Ref.
βTi	cI2, Im$\bar{3}$m, W	a_0 = 0.33112	[48]
αTi	hP2, P6$_3$/mmc, Mg	a_0 = 0.29503, c_0 = 0.46810	[48]
Ti_3Al	hP8, P6$_3$/mmc, Ni_3Sn	a_0 = 0.5765, c_0 = 0.4625	[49]
TiAl	tP4, P4/mmm, AuCu	a_0 = 0.4000, c_0 = 0.4075	[50]
TiAl (1d-APS)	one-dimensional, tetragonal ordered superstructures of AuCu P4/mmm, tP28, Ti_2Al_5	a_0 = 0.39053, c_0 = 2.91921	[51]
$TiAl_2$	tI24, I4$_1$/amd, $HfGa_2$	a_0 = 0.3971, c_0 = 2.4312	[52]
$TiAl_3$ (h)	tI8, I4/mmm, $TiAl_3$ (h)	a_0 = 0.3849, c_0 = 0.8610	[53]
Ti_5Si_3	hP16, P6$_3$/mmc, Mn_5Si_3	a_0 = 0.7452, c_0 = 0.5142	[54]

in Bragg-Brentano geometry in the range of 20 ° < 2θ < 120° using Co-Kα (λ = 0.178897 nm) radiation. Phases were identified using the X′Pert HighScore software together with the Powder Diffraction File ™ (PDF-2) provided from the International Center for Diffraction Data (ICDD) [42]. Lattice constants were calculated using TOPAS (Bruker AXS-Version 5). Compositions of the coexisting phases were established with EPMA (JEOL JXA-8100) using metallographic sections. To check the presence of any impurities, qualitative analyses were performed at 15 kV, 400 nA with a beam width of 3 µm. For quantitative analysis, standards of the pure elements have been used and analyses were performed at 15 kV, 20 nA with a focused beam. At least 12 measurements for each phase were carried out at least at five different places of the samples. Final compositions were obtained through ZAF matrix correction. In a few cases, specifically for samples annealed at 800 °C, phases were so fine-scaled that within the spatial resolution of the EPMA a fraction of the measured composition may come from neighbouring or underlying grains of another phase. In those cases, all analyses were plotted in a Gibbs triangle and only those data, which corresponded to the very end of a tie-line or the corners of a tie-triangle, i.e. the extreme values, were considered as equilibrium compositions. For these extreme values, no standard deviation can be given. Phase transformation temperatures were measured on bulk samples by DTA (NETZSCH STA 449 F3 Jupiter, NETZSCH DSC 404 C) under a stream of pure Ar and using alumina crucibles. Samples in as-cast and heat-treated condition were heated up to a maximum of about 1400 °C for at least two times and cooled down to room temperature at 10 K/min. Transformation temperatures were evaluated from the first heating cycle. By calibrating with the melting temperatures of pure elements, the experimental uncertainty was ± 2 °C.

3. Results and discussion

To establish the partial isothermal sections, compositions of the phase boundaries in the binary systems were taken from recent assessments. For Ti–Al the updated version [43] of the comprehensive assessment by Schuster & Palm [39] is chosen. The update settles the dispute about the peritectoid or congruent formation of Ti_3Al. While experiments show a peritectoid formation of Ti_3Al, all CALPHAD calculations predict a congruent formation of Ti_3Al. As detailed in [43], also the CALPHAD calculations show the peritectoid reaction αTi + βTi ↔ Ti_3Al at 1200 °C, if substitutional vacancies are included in the CALPHAD calculations. In consequence, the phase field of αTi is interrupted between 1170 and 1200 °C by the equilibrium βTi + Ti_3Al, i.e. no continuous phase field of αTi exists up to the melt. The Ti—Si binary was adopted from the latest thermodynamic assessment by Fiore et al. [44]. They conclude that the long ongoing debate whether the line compound Ti_3Si exists between the Ti solid solution and Ti_5Si_3 or whether this phase is stabilised by impurities cannot be settled from the existing evidence. The Al—Si binary is taken from Lukas & Lebrun [45]. It is a simple eutectic system containing no intermetallic phases.

The partial isothermal sections determined here comprise compositions up to 70 at% Al and 40 at% Si. The crystallographic data of the solid phases observed within this composition range are listed in Table 2. No ternary phase was detected within the investigated temperature and composition range. Additionally, Ti_3Si (tp32, P4$_2$/n [44,46]), whose existence is still under debate [44], was not detected in the present investigation. This phase was observed in the Ti–Al–Si system by Li et al. [30] and Gupta [26], but not in other studies [15,16,18,19,32,36,47]. Nevertheless, investigated compositions in the present work could be outside the composition range where equilibria with this phase may occur. Therefore, phase equilibria with Ti_3Si are indicated by dashed tie-triangle.

Comparison with the liquidus projection [27] shows that all alloy compositions are located within the primary field of high-melting Ti_5Si_3 (T_m = 2130 °C), except S7. Therefore, S1-S6 contained varying amounts of large idiomorphic grains of primary Ti_5Si_3 in the as-cast state. These grains are too big to equilibrate within reasonable annealing times. Therefore, all compositions measured by EPMA were

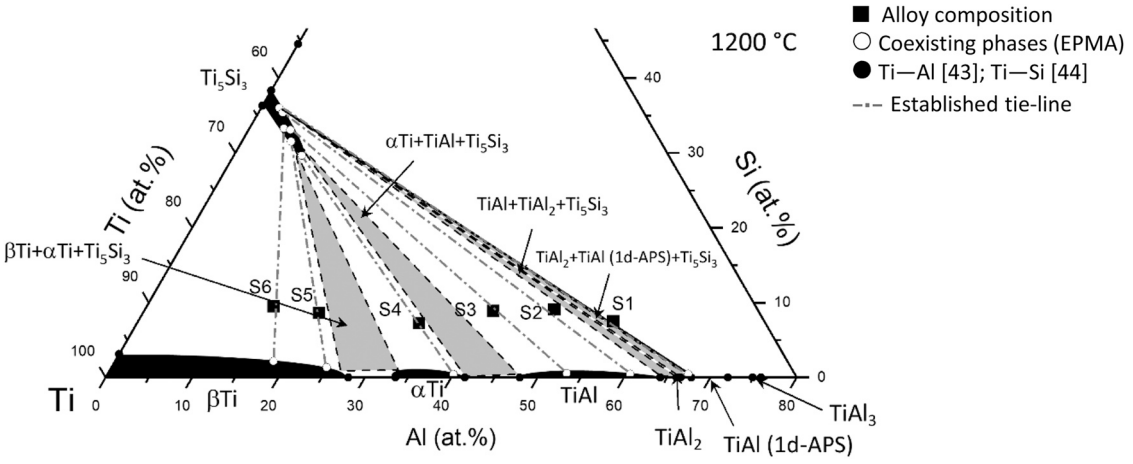

Fig. 1. Partial Ti—Al—Si isothermal section at 1200 °C.

Table 3
Compositions of coexisting phases measured with EPMA; figures for HT denote length of heat-treatment and figures shown in bold are extreme values (see text); n.d.: not determined.

Temp.	1200 °C				1100 °C				1000 °C			
Alloy	Phases	Ti	Al	Si	Phases	Ti	Al	Si	Phases	Ti	Al	Si
HT (h)	24				165				1000			
S1	Ti_5Si_3	61.9 ± 0.4	2.1 ± 0.4	36.0 ± 0.4	Ti_5Si_3	62.2 ± 0.2	1.1 ± 0.3	36.7 ± 0.2	Ti_5Si_3	61.2 ± 0.2	1.5 ± 0.4	37.3 ± 0.5
	TiAl (1d-APS)	32.3 ± 0.6	67.2 ± 0.6	0.5 ± 0.1	TiAl (1d-APS)	30.1 ± 0.2	69.6 ± 0.2	0.3 ± 0.04	$TiAl_3$	26.7 ± 0.5	72.7 ± 0.7	0.6 ± 0.2
					$TiAl_2$	34.6 ± 0.2	65.0 ± 0.2	0.4 ± 0.04	$TiAl_2$	34.6 ± 0.4	65.0 ± 0.4	0.4 ± 0.1
HT* (h)	24				200				1000			
S2	Ti_5Si_3	61.8 ± 0.3	2.8 ± 0.6	35.4 ± 0.5	Ti_5Si_3	61.2 ± 0.5	3.2 ± 0.5	35.6 ± 0.2	Ti_5Si_3	61.5 ± 0.5	3.9 ± 0.7	34.6 ± 0.5
	TiAl	39.0 ± 0.4	60.5 ± 0.4	0.5 ± 0.06	$TiAl_2$	34.8 ± 0.5	65.0 ± 0.5	0.2 ± 0.1	$TiAl_2$	35.1 ± 0.5	64.6 ± 0.6	0.3 ± 0.1
					TiAl	38.8 ± 0.4	60.8 ± 0.4	0.4 ± 0.1	TiAl	42.3 ± 0.4	57.5 ± 0.4	0.2 ± 0.1
HT* (h)	24				200				1000			
S3	Ti_5Si_3	62.1 ± 0.3	4.9 ± 0.5	33.1 ± 0.5	Ti_5Si_3	61.8 ± 0.2	4.0 ± 0.2	34.2 ± 0.3	Ti_5Si_3	61.2 ± 0.5	7.1 ± 0.7	31.7 ± 0.7
	TiAl	46.4 ± 0.3	53.1 ± 0.4	0.5 ± 0.2	TiAl	46.0 ± 0.3	53.7 ± 0.3	0.3 ± 0.04	TiAl	45.5 ± 0.3	54.1 ± 0.3	0.4 ± 0.1
HT* (h)	24				200				1000			
S4	Ti_5Si_3	62.5 ± 0.2	7.7 ± 0.6	29.8 ± 0.6	Ti_5Si_3	62.8 ± 0.3	6.7 ± 0.6	30.5 ± 0.6	Ti_5Si_3	62.4 ± 0.3	7.4 ± 0.5	30.2 ± 0.3
	αTi	59.6 ± 0.3	40.0 ± 0.3	0.4 ± 0.04	TiAl	54.6 ± 0.6	45.2 ± 0.6	0.2 ± 0.01	TiAl	53.3 ± 0.3	46.5 ± 0.3	0.2 ± 0.1
					Ti_3Al	61.8 ± 0.4	37.8 ± 0.4	0.4 ± 0.04	Ti_3Al	64.0 ± 0.7	35.5 ± 0.7	0.5 ± 0.1
HT* (h)	24				200				1000			
S5	Ti_5Si_3	62.8 ± 0.4	5.7 ± 0.2	31.5 ± 0.5	Ti_5Si_3	62.9 ± 0.2	5.4 ± 0.2	31.7 ± 0.3	Ti_5Si_3	62.8 ± 0.4	5.9 ± 0.2	31.3 ± 0.5
	βTi	73.8 ± 0.3	24.9 ± 0.2	1.3 ± 0.3	Ti_3Al	74.0 ± 0.4	24.5 ± 0.3	1.5 ± 0.2	Ti_3Al	73.6 ± 0.4	24.9 ± 0.2	1.5 ± 0.5
HT* (h)	24				200				1000			
S6	Ti_5Si_3	62.7 ± 0.3	4.0 ± 0.4	33.3 ± 0.5	Ti_5Si_3	62.9 ± 0.2	3.5 ± 0.3	33.6 ± 0.4	Ti_5Si_3	63.0 ± 0.2	3.5 ± 0.8	33.5 ± 0.8
	βTi	79.7 ± 0.4	18.3 ± 0.4	2.0 ± 0.3	βTi	80.8 ± 0.4	17.8 ± 0.4	1.4 ± 0.04	Ti_3Al	78.1 ± 0.6	20.1 ± 0.7	1.8 ± 0.2
									αTi	82.0 ± 0.5	17.1 ± 0.5	0.9 ± 0.03
HT* (h)									1000			
S7									Ti_5Si_3	62.7 ± 0.4	2.0 ± 0.3	35.3 ± 0.5
									αTi	86.3 ± 0.2	12.4 ± 0.2	1.3 ± 0.1

Temp. Alloy	900 °C				800 °C			
	Phases	Ti	Al	Si	Phases	Ti	Al	Si
HT* (h)	1000				1000			
S1	Ti_5Si_3	61.4 ± 0.4	2.2 ± 0.5	36.4 ± 0.4	Ti_5Si_3	**62.1**	**2.0**	**35.9**
	$TiAl_3$	n.d.	n.d.	n.d.	$TiAl_3$	**26.0**	**73.1**	**0.9**
	$TiAl_2$	34.6 ± 0.3	65.2 ± 0.3	0.2 ± 0.1	$TiAl_2$	**34.0**	**65.8**	**0.2**
HT* (h)	1504				1000			
S2	Ti_5Si_3	61.8 ± 0.2	2.9 ± 0.1	35.3 ± 0.2	Ti_5Si_3	**61.9**	**3.1**	**35.0**
	$TiAl_2$	35.7 ± 0.2	64 ± 0.2	0.3 ± 0.1	$TiAl_2$	**35.0**	**64.8**	**0.2**
	TiAl	43.5 ± 0.3	56.3 ± 0.3	0.2 ± 0.1	TiAl	44.6 ± 0.2	54.5 ± 0.5	0.9 ± 0.2
HT* (h)	1504				1000			
S3	Ti_5Si_3				Ti_5Si_3	62.5 ± 0.1	5.1 ± 0.3	32.4 ± 0.3
	TiAl				TiAl	46.1 ± 0.2	53.1 ± 0.3	0.8 ± 0.1
HT* (h)	1000				1000			
S4	Ti_5Si_3	63.0 ± 0.3	6.5 ± 0.3	30.5 ± 0.4	Ti_5Si_3	62.6 ± 0.2	8.0 ± 0.7	29.4 ± 0.8
	TiAl	53.8 ± 0.5	46.0 ± 0.6	0.2 ± 0.1	TiAl	**54.1**	**45.7**	**0.2**
	Ti_3Al	65.1 ± 0.4	34.5 ± 0.5	0.4 ± 0.2	Ti_3Al	**64.4**	**34.1**	**1.5**
HT* (h)	1000				1000			
S5	Ti_5Si_3	63.3 ± 0.3	5.9 ± 0.4	30.8 ± 0.5	Ti_5Si_3	62.8 ± 0.3	5.6 ± 0.2	31.6 ± 0.4
	Ti_3Al	74.6 ± 0.5	24.1 ± 0.5	1.3 ± 0.1	Ti_3Al	74.5 ± 0.3	24.1 ± 0.3	1.4 ± 0.1
HT* (h)	1000				1000			
S6	Ti_5Si_3	62.9 ± 0.2	4.7 ± 0.4	32.4 ± 0.4	Ti_5Si_3	62.0 ± 0.2	4.7 ± 0.1	33.3 ± 0.2
	Ti_3Al	78.2 ± 0.3	20.2 ± 0.3	1.6 ± 0.1	Ti_3Al	**78.5**	**20.1**	**1.4**
	αTi	83.2 ± 0.3	16.0 ± 0.2	0.8 ± 0.1	αTi	**83.0**	**15.5**	**1.5**
HT* (h)	1000				1000			
S7	Ti_5Si_3	63.7 ± 0.8	2.4 ± 0.3	33.9 ± 0.8	Ti_5Si_3	63.5 ± 1.1	1.8 ± 0.4	34.7 ± 1.1
	αTi	86.8 ± 0.2	12.4 ± 0.2	0.8 ± 0.1	αTi	87.1 ± 0.7	12.3 ± 0.7	0.6 ± 0.1

obtained from small, spherical Ti_5Si_3 grains, which are assumed to have formed at the annealing temperatures.

3.1. Partial isothermal section at 1200 °C

Fig. 1 depicts the partial isothermal section at 1200 °C. All investigated alloys are located within two-phase fields at this temperature. The compositions of coexisting phases measured with EPMA are summarised in Table 3 and identification of the phases by XRD is shown in Table 4. All binary Ti–Al phases show a limited solid solubility for Si, while the maximum Al content observed in Ti_5Si_3 is about 8 at%. It is noted that in alloys where βTi is stable at 1200 °C, αTi is observed at room temperature, instead. The βTi ↔ αTi transformation in Ti—Al alloys cannot be suppressed even by quenching [41,49,55] and also not in Ti—Al—Si alloys [11,22]. Likewise, the ordering reaction αTi ↔ Ti_3Al (α_2) cannot be suppressed during cooling in binary Ti—Al alloys, even by quenching the alloys to room temperature [49,56]. The same has been observed for the Ti—Al—Si alloys [22]. Finally, Al-rich TiAl cannot be preserved by quenching, but forms a sequence of long-periodic one-dimensional antiphase domain structures during cooling, denoted as 1d-APS [57]. Depending on the composition, different crystallographic structures are observed at room temperature, identified as Ti_2Al_5 in the present case.

In Fig. 2 the present isothermal section is compared with previously reported data [17–22,24,58,59]. The outline of the βTi phase field at 1200 °C has been investigated before [17,19,22] and the present investigation agrees with the previous ones in that the solid solubility for Si in βTi decreases with increasing Al content. Quantitatively, the solid solubility for Si in βTi is somewhat higher than previously determined, e.g. 2.0 at% Si at about 20 at% Al compared to about 1.5 at% Si [17,22]. Only Schob et al. [17] investigated a more extended composition range at 1200 °C. They observed an extended

Table 4
Lattice constants of the constituent phases; αTi* denotes formation from βTi during quenching to room temperature.

Alloy	1200 °C			1100 °C			1000 °C		
	Phase	Lattice constant (nm)		Phase	Lattice constant (nm)		Phase	Lattice constant (nm)	
		a_0	c_0		a_0	c_0		a_0	c_0
S1	Ti_5Si_3	0.74596 (1)	0.51470 (2)	Ti_5Si_3	0.74545(2)	0.51478(1)	Ti_5Si_3	0.74533 (2)	0.51495 (2)
	Ti_2Al_5	0.393519 (1)	2.8932 (1)	Ti_2Al_5	0.39158(2)	2.9125(3)	$TiAl_3$	0.38523 (2)	0.86009 (6)
				$TiAl_2$	0.39704(3)	2.4310(7)	$TiAl_2$	0.397041(7)	2.43098(7)
S2	Ti_5Si_3	0.74641(1)	0.51520 (1)	Ti_5Si_3	0.74644(1)	0.51521(2)	Ti_5Si_3	0.74688(2)	0.51554(2)
	TiAl	0.39782(1)	0.40593 (2)	$TiAl_2$	0.39848(3)	2.4373(6)	$TiAl_2$	0.39737(2)	2.4317(2)
				TiAl	0.4020(5)	0.3974(3)	TiAl	0.39882(3)	0.40796(3)
S3	Ti_5Si_3	0.74794 (1)	0.51637 (2)	Ti_5Si_3	0.74778(5)	0.51611(4)	Ti_5Si_3	0.74767 (2)	0.51605 (2)
	TiAl	0.39846 (1)	0.40773 (2)	TiAl	0.40412(6)	0.3978 (1)	TiAl	0.39855 (2)	0.40844 (3)
S4	Ti_5Si_3	0.74991 (2)	0.51824 (2)	Ti_5Si_3	0.75062(9)	0.51816(8)	Ti_5Si_3	0.75053 (2)	0.51768 (2)
	αTi	0.29138(1)	0.46222(2)	TiAl	0.4030(1)	0.3955(1)	TiAl	0.40650(4)	0.39795(3)
				Ti_3Al	0.57691(8)	0.4628 (1)	Ti_3Al	0.56160(7)	0.46279(3)
S5	Ti_5Si_3	0.74790 (2)	0.51721(1)	Ti_5Si_3	0.74878(9)	0.51695(8)	Ti_5Si_3	0.74958(8)	0.51737(8)
	αTi*	0.28974 (1)	0.46384 (2)	Ti_3Al	0.5770 (1)	0.4646 (2)	Ti_3Al	0.57913(6)	0.46403(4)
S6	Ti_5Si_3	0.74758 (3)	0.51629 (2)	Ti_5Si_3	0.7483(1)	0.5164(1)	Ti_5Si_3	0.74818 (3)	0.51566 (3)
	αTi*	0.28997 (1)	0.46465 (2)	**αTi***	0.29157 (5)	0.4658 (1)	Ti_3Al	0.5796 (1)	0.4648(7)
							αTi	0.29171(5)	0.4673 (1)
S7							Ti_5Si_3	0.74771 (2)	0.51543 (2)
							αTi	0.29231 (1)	0.46629 (3)

Lattice constants of the constituent phases in the annealed Ti—Al—Si alloys

Alloy	900 °C			800 °C		
	Phase	Lattice constant (nm)		Phase	Lattice constant (nm)	
		a_0	c_0		a_0	c_0
S1	Ti_5Si_3	0.74522 (1)	0.51473 (2)	Ti_5Si_3	0.74533 (5)	0.51529(6)
	$TiAl_3$	0.38510(7)	0.86017 (5)	$TiAl_3$	0.38524(7)	0.86050(5)
	$TiAl_2$	0.39682(1)	2.43124 (7)	$TiAl_2$	0.39701 (7)	2.43147(2)
S2	Ti_5Si_3	0.74531(4)	0.51500(4)	Ti_5Si_3	0.74695(4)	0.51569(4)
	$TiAl_2$	0.37579(2)	2.56815(8)	$TiAl_2$	0.39791(3)	2.4425(3)
	TiAl	0.39701(2)	0.40527(3)	TiAl	0.39835(5)	0.40544(9)
S3	Ti_5Si_3	0.74675(4)	0.51548(4)	Ti_5Si_3	0.74806(6)	0.51642(6)
	TiAl	0.39800(2)	0.40708(4)	TiAl	0.39919(3)	0.40768(5)
S4	Ti_5Si_3	0.75022(5)	0.51792(5)	Ti_5Si_3	0.75078(5)	0.51828(5)
	TiAl	0.40073(4)	0.40579(6)	TiAl	0.40080(4)	0.40622(6)
	Ti_3Al	0.57690(5)	0.46295(6)	Ti_3Al	0.57760(5)	0.46354(7)
S5	Ti_5Si_3	0.74954(7)	0.51713(6)	Ti_5Si_3	0.74997(7)	0.51753(7)
	Ti_3Al	0.57951(5)	0.46424(4)	Ti_3Al	0.57921(5)	0.46423(4)
S6	Ti_5Si_3	0.74704 (2)	0.51609(2)	Ti_5Si_3	0.7486(3)	0.5169(3)
	Ti_3Al	0.5787(2)	0.4646(1)	Ti_3Al	0.58072(3)	0.46641(3)
	αTi	0.29188(5)	0.4668(2)	αTi	0.29131(1)	0.46396(2)
S7	Ti_5Si_3	0.74713(6)	0.51555(6)	Ti_5Si_3	0.74711(8)	0.51557(8)
	αTi	0.29274(2)	0.46651(3)	αTi	0.29272(3)	0.46648(4)

homogeneity range for Ti_3Al, denoted as $Ti_{3-2}Al$ in their investigation, which showed a solid solubility of up to about 6 at% Si. However, by now it is clear that Ti_3Al exists only below 1200 °C, as it forms at that temperature on cooling by the peritectic reaction βTi + αTi ↔ Ti_3Al [39,43]. Instead of Ti_3Al, αTi is stable in that composition range at 1200 °C and its solubility for Si at that temperature is limited to about 0.5 at% (Fig. 1). Additionally, as $TiAl_2$ had not been considered, phase equilibria in the more Al-rich part differ in [17] from present work (Fig. 2).

3.2. The partial isothermal section at 1100 °C

The partial isothermal section at 1100 °C is shown in Fig. 3**a**. At this temperature, alloys S1, S2, and S4 show three-phase equilibria (Table 3). Compared to the isothermal section at 1200 °C, Ti_3Al is

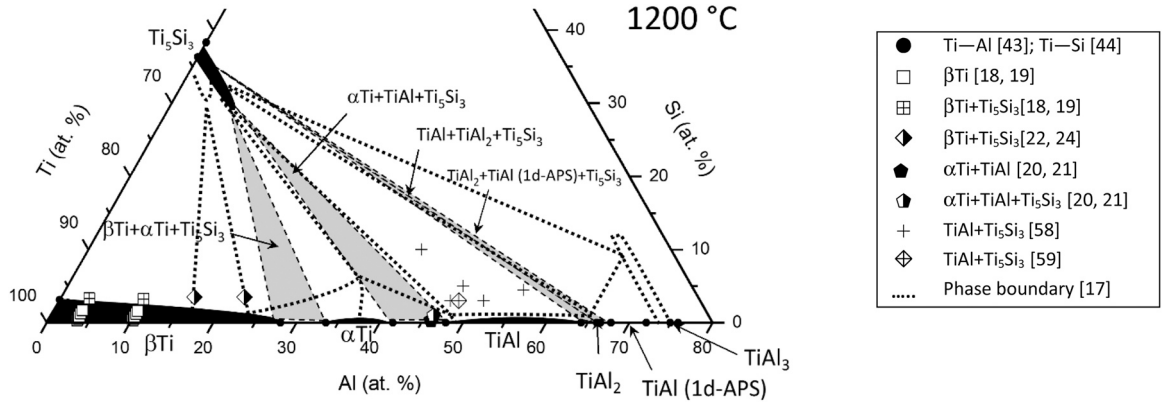

Fig. 2. Partial Ti—Al—Si isothermal section at 1200 °C in comparison to experimental results from literature.

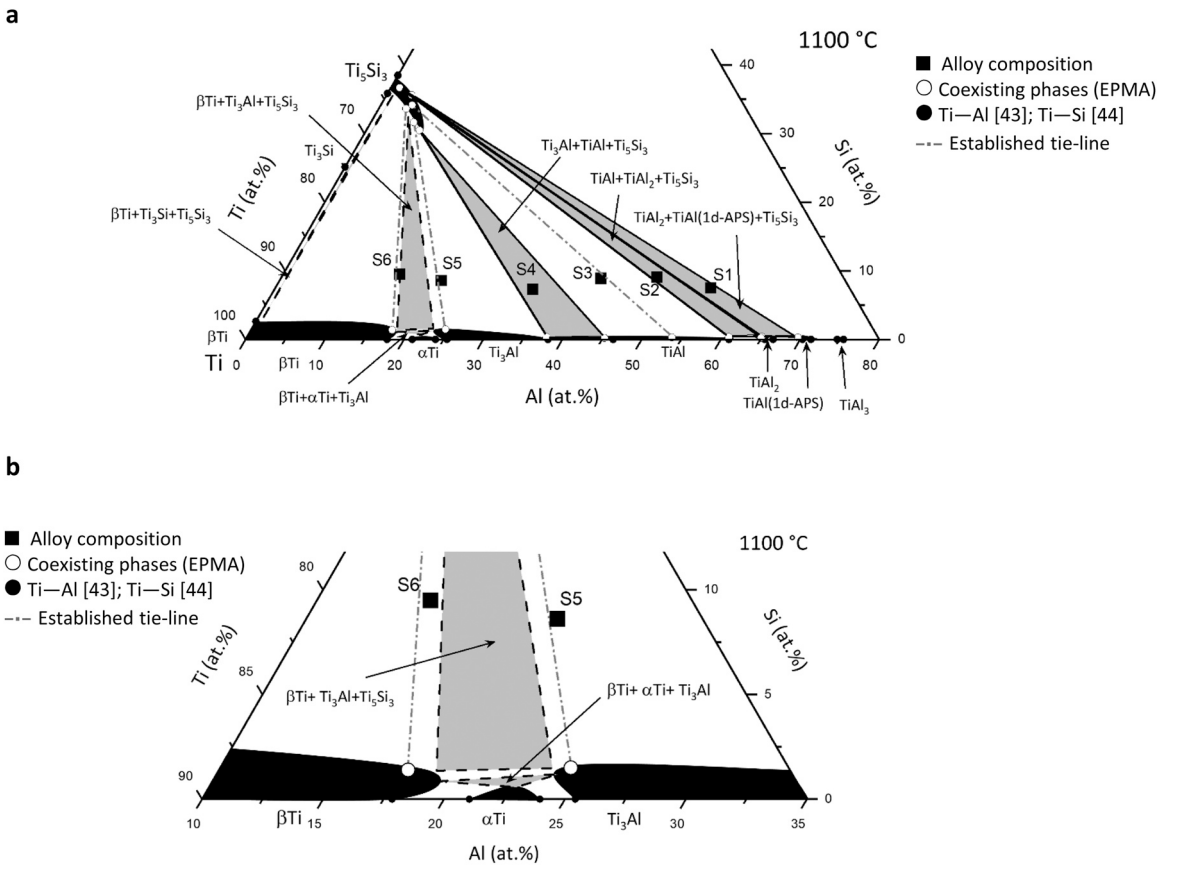

Fig. 3. a- Partial Ti-Al-Si isothermal section at 1100 °C. **b-** Enlarged part of the 1100 °C isotherm showing phase equilibria with αTi.

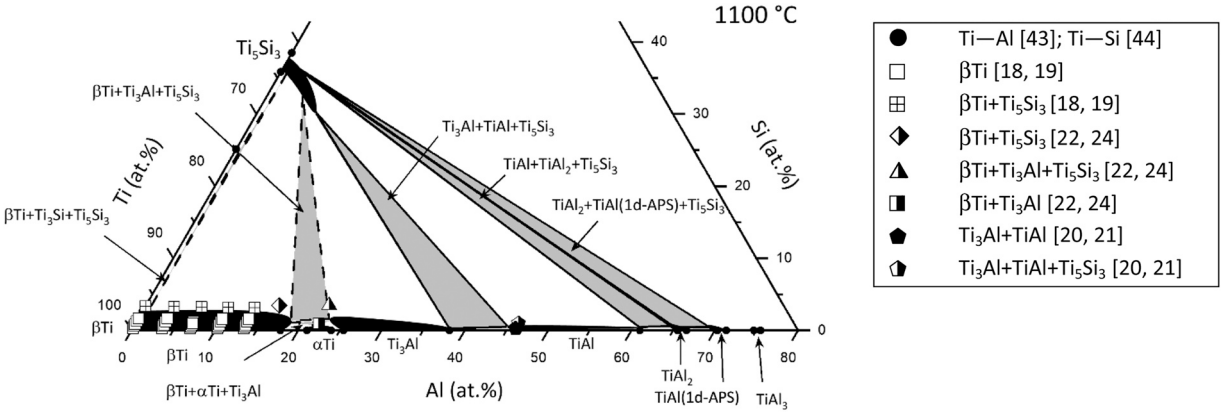

Fig. 4. Partial Ti—Al—Si isothermal section at 1100 °C with additional experimental results from literature.

present at 1100 °C and is in equilibrium with Ti_5Si_3, like βTi, TiAl, and $TiAl_2$. No equilibrium between αTi and Ti_5Si_3 is observed, in agreement with the DTA results, which show that αTi + Ti_5Si_3 does not exist between 1095 and 1152 °C (see below). This finding is in agreement with Azevedo & Flower [22,24], who observed the three-phase equilibrium βTi + Ti_3Al + Ti_5Si_3 at 1100 °C. It may look strange, that the phase equilibrium αTi + Ti_5Si_3 is observed at higher and lower temperatures, but not at 1100 °C. However, that at 1100 °C the equilibrium αTi + βTi + Ti_3Al is observed instead (Fig. 3**b**) is in full agreement with the binary Ti–Al system, where no continuous phase field of αTi up to the melt exists. At 1100 °C previous data concentrated on the Ti corner [18–22,24] and Fig. 4 shows that these are in good agreement with the present ones.

3.3. The partial isothermal section at 1000 °C

For the determination of the phase equilibria at 1000 °C samples had initially been heat treated only for 100 h. This duration showed to be too short to reach equilibrium and therefore all alloys were annealed for 1000 h, from which the partial isothermal section in Fig. 5 was established. Microstructures and XRD analyses of the alloys heat-treated at 1000 °C/1000 h are shown in Figs. 6, 7. In alloys S1-S4 (Fig. 6) large, idiomorphic grains of Ti_5Si_3 are observed. These are primary precipitates, which formed in the melt (Fig. 6**b**). As described above, no EPMA was performed on these primary grains, because they are still not in equilibrium after annealing for 1000 h, and hence measurements were only performed on small, spherical

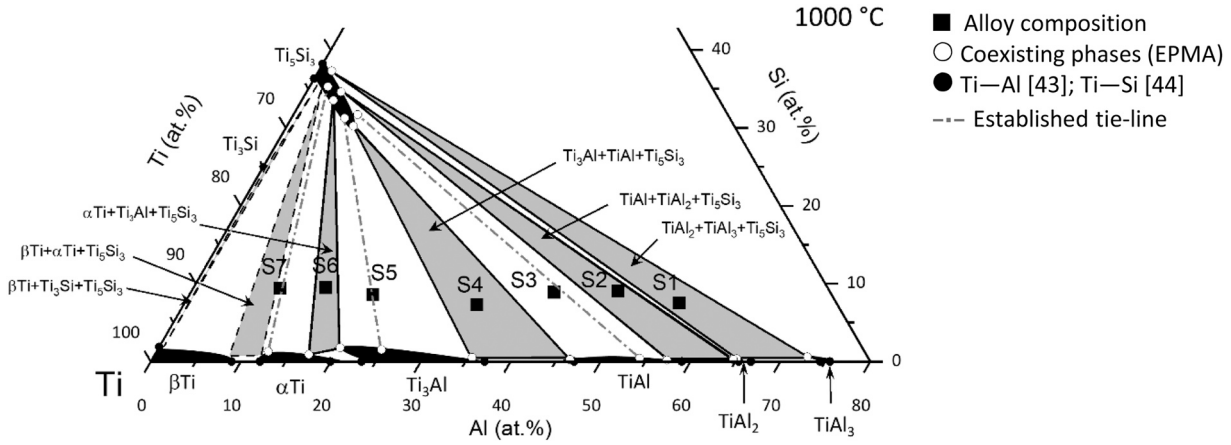

Fig. 5. Partial Ti—Al—Si isothermal section at 1000 °C.

Ti_5Si_3 grains which are present in the alloys besides the large idiomorphic grains (Fig. 6**b**).

The partial isothermal section in Fig. 5 agrees qualitatively with the one determined by Liu et al. [27]. However, phase equilibria among the phases Ti_5Si_3, βTi, αTi, Ti_3Al, and TiAl were not determined in [27] and were therefore shown by dashed lines. Liu et al. [27] reported a solid solubility of Al of 11 at%. in Ti_5Si_3, which is only about 7 at% according to the present investigation. Additionally, the shape of the Ti_5Si_3 single-phase field in [27] is different in that it stretches along a constant Ti:Si ratio, while the one shown in Fig. 5 is more inclined towards the Ti—Al side, indicating a more pronounced substitution of Si by Al than assumed in [27]. That the present finding is more likely is corroborated by the fact that the measured Al content in Ti_5Si_3 at the three-phase equilibrium Ti_5Si_3 + $TiAl_2$ + $TiAl_3$ was 2.5–3.9 at% in [27] (1.5 at% Al determined in here), while, due to the shape of their single-phase field, it is shown at 10 at% Al in their isothermal section.

The isothermal section established from diffusion couples by Gupta [26] differs considerably from the established partial isothermal section in Fig. 5. Gupta [26] found αTi, Ti_3Al and TiAl in equilibrium with Ti_3Si. There have been two other investigations of the Ti—Al—Si system at 1000 °C, both focussing on the Ti corner. As in the present investigation, they also found αTi, Ti_3Al and TiAl in equilibrium with Ti_5Si_3 instead of Ti_3Si (Fig. 5) [15,16,22,24]. Additionally, Gupta observed Ti_9Al_{23}, which is no binary Ti—Al phase [39]. According to compositions reported in [26,60] it seems that this "phase" lies within the extended solid solubility range of $Ti(Al,Si)_3$.

3.4. Partial isothermal sections at 900 °C and 800 °C

The partial isothermal sections at 900 °C (Fig. 8) and 800 °C (Fig. 10) show the same phase equilibria as at 1000 °C. Alloys S1, S2, S4, and S6 all lie within different three-phase fields from which the tie-triangles were determined. It is noted that in S1 annealed at 900 °C $TiAl_3$ was observed by EPMA and identified by XRD (Table 4), but that all particles were too small for quantitative EPMA.

For 900 °C phase equilibria are in qualitative agreement with previous investigations of the Ti corner at this temperature [15,16,22,24]. In the Ti/Al—Si diffusion couple analysed by Gupta at 900 °C, no Ti_3Si was observed, while Ti_9Al_{23} was detected again [26]. More recently, complete isothermal sections were calculated for the temperature range 450–900 °C [31,61]. In Fig. 9 the calculated isothermal section for 900 °C by Li et al. [31] is compared to the present one. calculated and experimentally determined phase equilibria are in qualitative agreement. As the calculation is based on a different description of the binary Ti—Al system and as except for βTi no solid solubility ranges for the third component, specifically not for Al in Ti_5Si_3, have been calculated, calculated and experimental determined phase equilibria are somewhat shifted against each other (Fig. 9). The most prominent difference is the extent of αTi + βTi + Ti_3Si, which has not been determined in the present investigation, but which should be positioned much nearer to the Ti—Si side than shown in the calculation according to [19], who studied the respective composition range at 900 °C in much detail.

At 800 °C Ti_3Si was again observed in a diffusion couple and therefore the existence of a three-phase field TiAl + Ti_3Al + Ti_3Si had been proposed [26]. According to the present investigation (Fig. 10), phase equilibria with Ti_5Si_3 are observed instead. This is in accordance with the investigation of the Ti corner at 800 °C [15,16] where also αTi + Ti_5Si_3 was observed, which rules out any phase equilibria of Ti_3Si with more Al rich phases.

3.5. DTA analyses

DTA was performed on all alloys in the as-cast condition and, where results have been ambiguous, additionally on samples equilibrated at 900 °C. Table 5 summarizes observed temperatures, allocation to certain reactions, and references for invariant reactions. Temperatures given in Table 5 are evaluated from the first heating if not noted otherwise, but those, for which error limits are given, have also been observed in second heating and/or cooling cycles.

S1 showed melting at 1386 °C, in excellent agreement with 1391 °C [27] and 1380–1390 °C [15] observed for alloys of comparable composition. The temperature has been attributed to the invariant reaction L + TiAl ↔ $TiAl_3$ + Ti_5Si_3 (U_3 in [27]). The strong signal at about 1100 °C is attributed to the reaction TiAl (1d-APS) + Ti_5Si_3 ↔ $TiAl_2$ + $TiAl_3$ + Ti_5Si_3. That the signal observed in the DTA is always stronger on cooling is in line that it stems from the eutectoid decomposition of TiAl (1d-APS). This reaction is listed in the reaction scheme in [15] as "U_{12}". No temperature for "U_{12}" had yet been determined, but as indicated in [15], the temperature should be higher than 977 °C as in the binary system [43], presumably because $TiAl_3$ is the only binary Ti—Al phase which shows a substantial solid solubility for Si [17,27]. The present investigation now shows that indeed the temperature is about 120 K higher than in the binary system. The signal observed in S1 on heating of the equilibrated sample at about 1194 °C is associated with the transition from the three-phase field TiAl (1d-APS) + $TiAl_2$ + Ti_5Si_3 to the two-phase field TiAl (1d-APS) + Ti_5Si_3, as the annealed sample consisted mainly out of $TiAl_2$, in agreement with Fig. 8. The temperature is also in good agreement with the dissolution temperature of $TiAl_2$ in the binary system (1215 °C [43]), which should not be much lower in the ternary system, as the solid solubility for Si in $TiAl_2$ is very limited

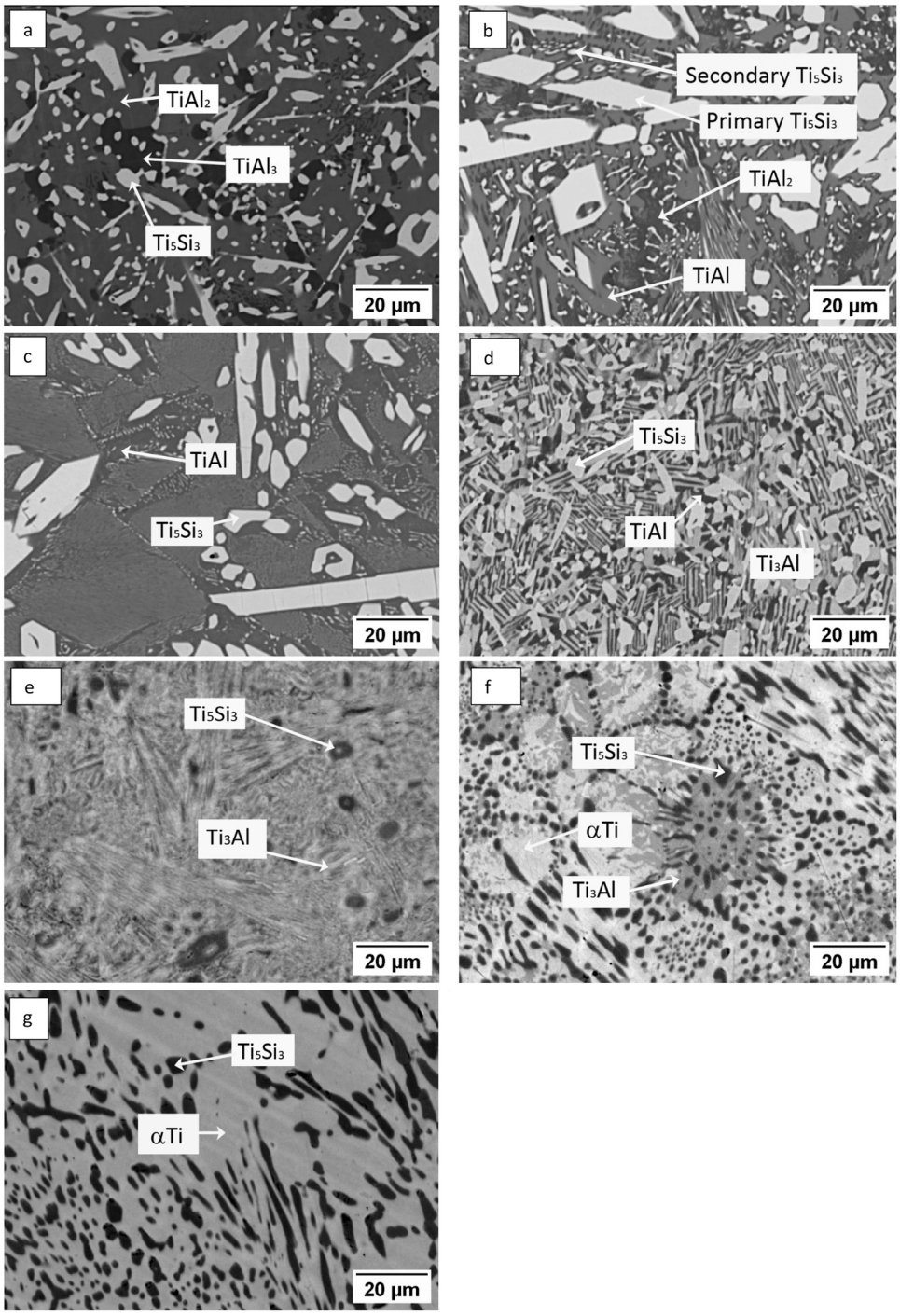

Fig. 6. Microstructures of the alloys a) S1; Ti-55Al-7.5Si (at%), b) S2; Ti-47.4Al-9.1Si, c) S3; Ti-40.4Al-8.9Si, d) S4; Ti-32.7Al-7.1Si, e) S5; Ti-20.4Al-8.6Si, f) S6; Ti-14.7Al-9.5Si, g) S7; Ti-9.7Al-9.6Si heat-treated 1000 °C/1000 h.

and actually 1216 °C have been observed for the stoichiometric ternary composition [32].

For S2 no signals were recorded during first heating (Table 5). A weak signal observed at 1143 °C during the second heating could indicate transition from TiAl + $TiAl_2$ + Ti_5Si_3 to TiAl + Ti_5Si_3. No signals were observed for S3 up to 1400 °C. In S4 the eutectoid reaction αTi + Ti_5Si_3 ↔ Ti_3Al + TiAl + Ti_5Si_3 is observed at 1110 °C, which is in excellent agreement with 1100 °C [27] and 1107 °C [15]. The two signals at 1325 °C and 1295 °C should be associated with the transition from βTi + Ti_5Si_3 to αTi + Ti_5Si_3 on cooling.

In S5, the peritectoid formation of Ti_3Al on cooling is observed at 1152 °C, which was observed at 1158 °C in [27]. A signal observed at 1170 °C in an alloy of nearly the same composition may stem from the same reaction [27]. The signal in S6 at about 1095 °C is associated with the peritectoid formation of αTi and a signal observed at 1090 °C in [27] in an alloy of nearly identical composition should be related to the same reaction. The signals in S7 at about 1080 °C and about 1030 °C are associated with crossing the αTi + βTi two-phase field, i.e. the formation of αTi and the dissolution of βTi on cooling, respectively.

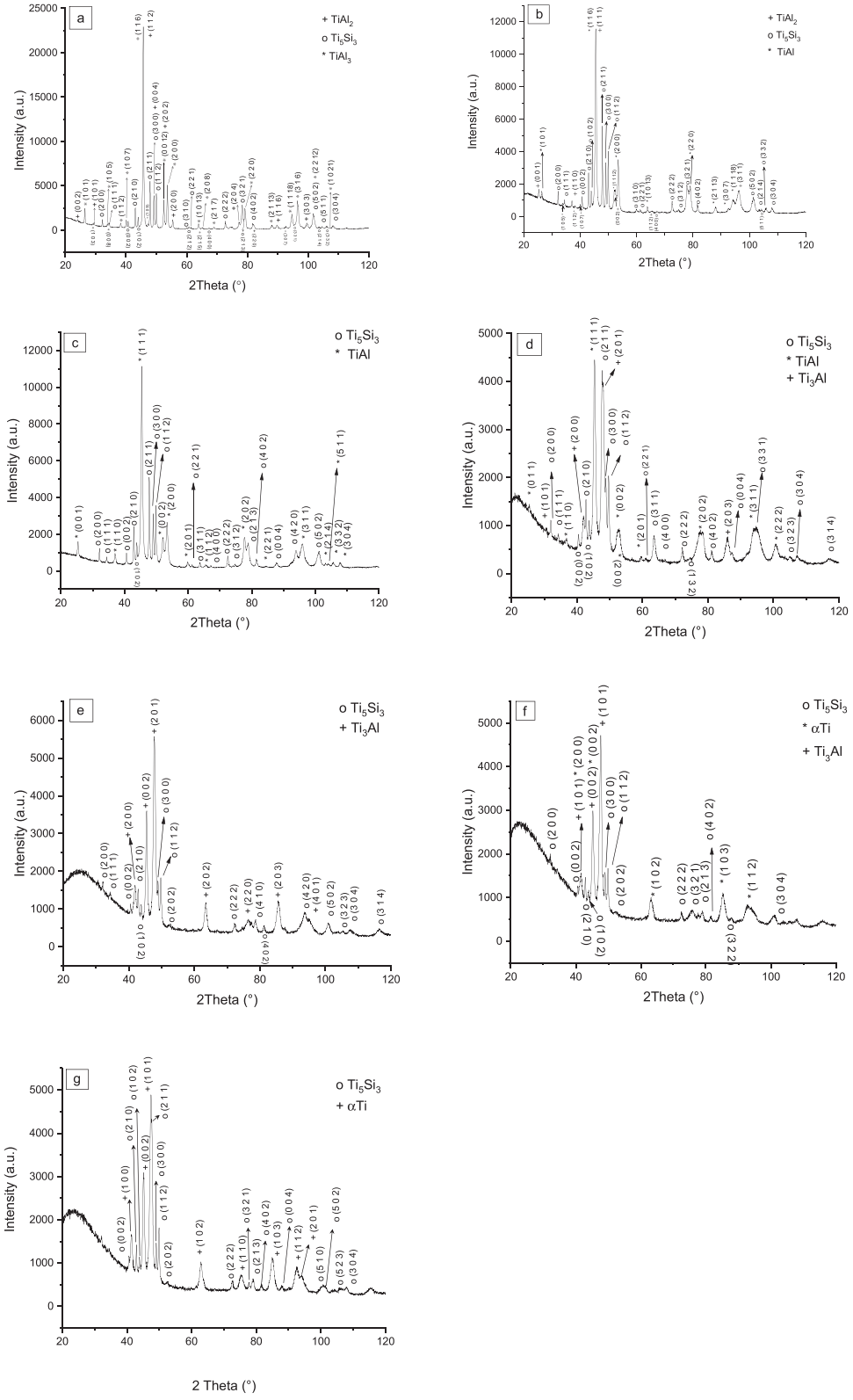

Fig. 7. XRD analyses of a) S1; Ti-55Al-7.5Si, b) S2; Ti-47.4Al-9.1Si, c) S3; Ti-40.4Al-8.9Si, d) S4; Ti-32.7Al-7.1Si, e) S5; Ti-20.4Al-8.6Si, f) S6; Ti-14.7Al-9.5Si, g) S7; Ti-9.7Al-9.6Si heat-treated 1000 °C/1000 h.

3.6. Vertical section at 9 at% Si

In order to check the consistency of the determined phase equilibria, a partial vertical section (Fig. 11) has been established from the intersections of the phase boundaries at 9 at% Si in Figs. 1, 3, 5, 8, 10 and the DTA results. It is noted that the actual Si content in the alloys deviates slightly from 9 at% Si (Table 1). Hence, some phase boundaries shown in Fig. 11 do not exactly match the temperatures determined by DTA (Table 5). Results from [15,16,27,62] for alloys with about 8 – 10 at% Si have been added for comparison and

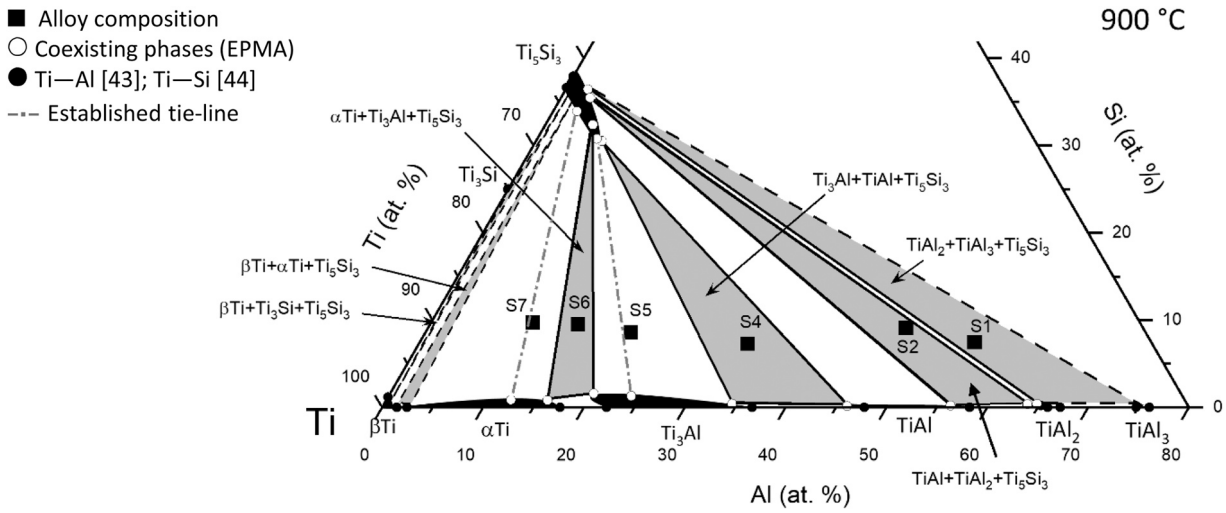

Fig. 8. Partial Ti—Al—Si isothermal section at 900 °C.

also to show continuation of phase boundaries up to the liquidus. As in the isothermal sections possible phase equilibria with Ti_3Si are indicated by dashed lines in Fig. 11.

Comparison of the vertical section and the actual phase content shows that only for one out of thirty-three samples there seems to be a discrepancy. According to Fig. 11, S4 should contain a minor amount of TiAl at 1200 °C, which could not be detected by EPMA or XRD. However, the composition of S4 is close to the αTi + Ti_5Si_3/αTi + TiAl + Ti_5Si_3 phase boundary and as S4 is the alloy with the lowest Si content (7.1 at., Table 1), the shift with respect to the vertical section at 9 at% Si should account for this discrepancy.

The outline of the vertical section resembles that of the binary Ti—Al system. The same invariant reactions are observed except that Ti_5Si_3 is additionally present in the ternary system. In Table 6 the determined temperatures of the invariant reactions are compared to those of the binary system. The peritectoid formation of Ti_3Al and of αTi occur at substantially lower temperatures than in the binary system, the eutectoid decomposition of TiAl(1d-APS) takes place at a much higher temperature in the ternary system, while the temperature of the eutectoid decomposition of αTi is little affected by the addition of Si.

Results from literature [15,16,27,47,62] have been added to the vertical section. It is noted that data taken from literature also do not always lie exactly on this vertical section, as many of the investigated alloys contained 10 at% Si. However, nearly all of the results for equilibrated samples [15,16] are in agreement with the phase boundaries shown in Fig. 11.

Bulanova et al. [16] presented a partial vertical section at 10 at% Si for Al contents between 10 and 40 at%, which differs in two points from the present one. Besides showing phase equilibria with Ti_3Si, though this phase was not detected in any of their samples, they show a continuous phase field for αTi + Ti_5Si_3. Obviously, the continuous phase field was assumed in agreement with the shape of the αTi phase field in the then-accepted Ti—Al binary system. However, in order to fit with their DTA results, they had to draw S-shaped phase boundaries, which is thermodynamically improbable. The DTA results from [16] would fit with the vertical section shown in Fig. 9, however assuming different phase transitions in some of the alloys.

Data from [15,27,47] were used in Fig. 11 to show how phase boundaries may continue up to the liquidus. 1570 °C for the temperature of the invariant reaction L (+ Ti_5Si_3) ↔ βTi (+ Ti_5Si_3) and 18 at% Al for the composition of L for the intersection of the eutectic line at 9 at% Si were adopted from [16]. This composition matches quite well with that calculated for a partial liquidus line (21 at% Al) [47] but is somewhat higher than 15 at% Al found in [27].

It is noted that phase boundaries extrapolated to lower temperatures are in good agreement with the isothermal section from Li et al. [30] at 700 °C.

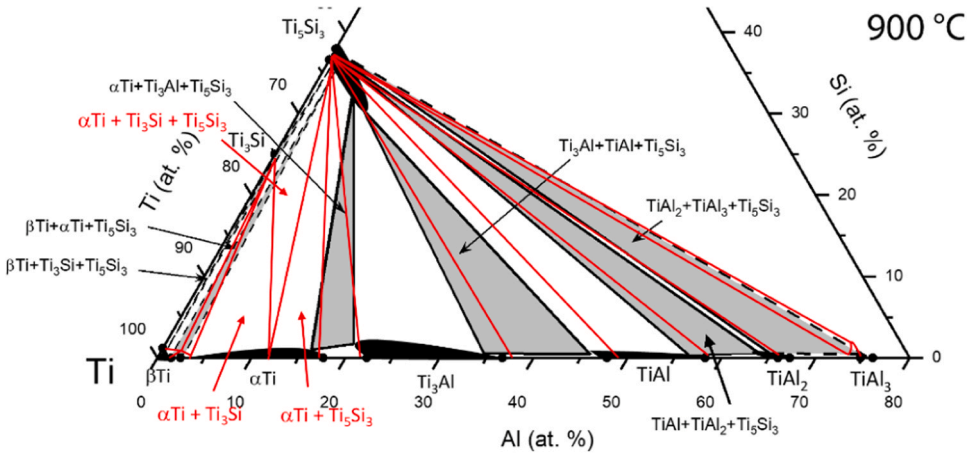

Fig. 9. Partial Ti—Al—Si isothermal section at 900 °C compared to the calculated one (in red) from [31].

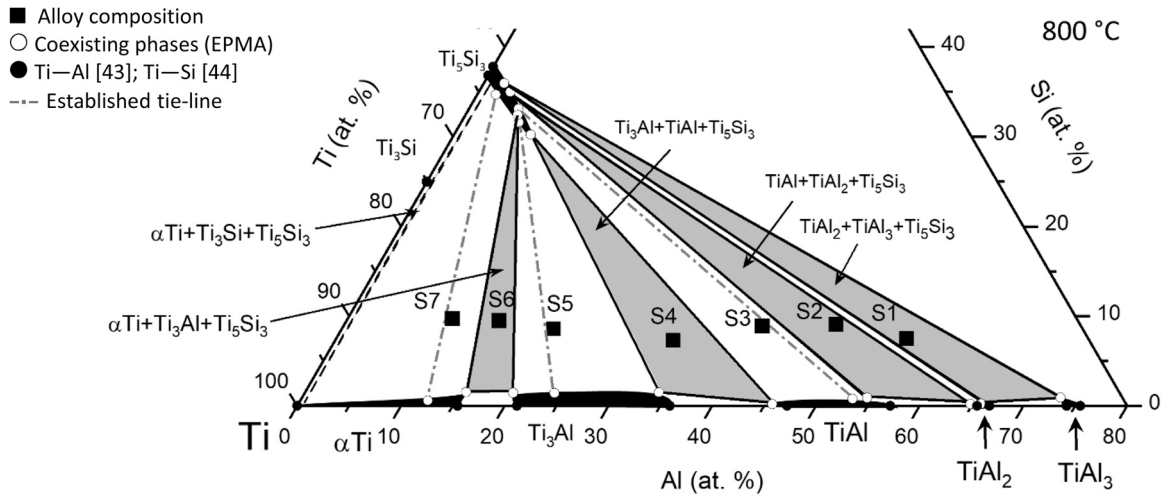

Fig. 10. Partial Ti—Al—Si isothermal section at 800 °C.

3.7. The solid solubility of Si in the binary Ti—Al phases

One of the main tasks of the current undertaking was to settle the discrepancy in published data about the solid solubility of Si in the binary Ti—Al phases. The comparison of the partial isotherms in Figs. 1, 3, 5, 8 shows that the solid solubility for Si in βTi increases with increasing temperature. At all temperatures, the solid solubility decreases with increasing Al content, in agreement with [15–19], and therefore the highest solid solubility is observed in binary Ti—Si at all temperatures. Also, the solid solubility of Si decreases steadily with increasing Al content, ruling out the thermodynamically improbable S-shape of the βTi phase boundary calculated in [23,24].

Fig. 12 illustrates the solid solubility of Si in αTi, Ti_3Al, TiAl, and $TiAl_2$ in dependence on temperature. Fig. 12 shows those compositions, for which no marked change in the Al content in dependence on temperature is observed. For αTi with about 12 at% Al (S7), the solid solubility for Si increases from 0.8 at% Si at 800 °C to 1.3 at% at 1000 °C. These data are in perfect agreement with those data determined by [18,19] for αTi with about 10 at% Al. The solid solubility of Si in αTi at a given temperature does also not change with the Al content, as shown in [18,19] for lower Al contents, and by comparison with data determined at higher Al contents for αTi in alloy S6. However, calculated isotherms in [22,24] show slight variations of the solubility for Si with the Al content.

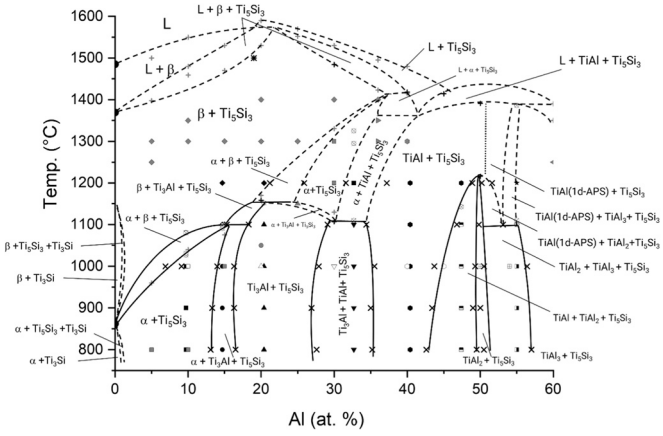

Fig. 11. Vertical section of Ti—Al—Si system at 9 at% Si with literature data.

Data for S5 show that the solid solubility of Si in Ti_3Al with about 25 at% Al is about 1.4 at% and that it does not change with temperature. It is therefore somewhat higher than in disordered αTi. The data are in excellent agreement with those measured in [22] and notably smaller than determined in [17,27].

In alloy S3 the solid solubility of Si in TiAl is about 0.5 at% and independent of temperature. This value agrees with compositions

Table 5
DTA results; reactions are listed with decreasing temperature; strength of the signals is indicated by ss (very strong), s (strong), and w (weak).

Alloy	Al (at%)	Si (at%)	Condition	Heated to °C	Signal (°C); strength	Reaction	Ref.
S1	55	7.5	900 °C/1504 h	1400	1386; ss	L + TiAl + Ti_5Si_3 ↔ $TiAl_3$ + Ti_5Si_3	[15,27]
					~1194; s	TiAl(1d-APS) + Ti_5Si_3 ↔ TiAl(1d-APS) + $TiAl_2$ + Ti_5Si_3	
					1110 ± 10; s	TiAl(1d-APS) + Ti_5Si_3 ↔ $TiAl_2$ + $TiAl_3$ + Ti_5Si_3	[15]
			As-cast	1300	1100 ± 1; s	TiAl(1d-APS) + Ti_5Si_3↔ $TiAl_2$ + $TiAl_3$ + Ti_5Si_3	[15]
S2	47.4	9.1	900 °C/1504 h	1350	1143; w	TiAl + Ti_5Si_3 ↔ TiAl + $TiAl_2$ + Ti_5Si_3	
			As-cast	1300	–		
S3	40.4	8.9	As-cast	1400	–		
S4	32.7	7.1	900 °C/1000 h	1400	1325 ± 4; s	βTi + Ti_5Si_3 ↔ αTi + βTi + Ti_5Si_3	
					1295 ± 5; s	αTi + βTi + Ti_5Si_3 ↔ αTi + Ti_5Si_3	
					1110 ± 5; s	αTi + Ti_5Si_3 ↔ Ti_3Al + TiAl + Ti_5Si_3	[15,27]
			As-cast	1300	1109 ± 1; s	αTi + Ti_5Si_3 ↔ Ti_3Al + TiAl + Ti_5Si_3	[15,27]
S5	20.4	8.6	As-cast	1300	1152 ± 2; s	βTi + αTi + Ti_5Si_3 ↔ Ti_3Al + Ti_5Si_3	[27]
S6	14.7	9.5	900 °C/1000 h	1300	1091 ± 5; s	βTi + Ti_3Al + Ti_5Si_3 ↔ αTi + Ti_5Si_3	
			As-cast	1300	1098 ± 1; s	βTi + Ti_3Al + Ti_5Si_3 ↔ αTi + Ti_5Si_3	
S7	9.7	9.6	900 °C/1000 h	1350	1080 ± 5; w	βTi + Ti_5Si_3 ↔ βTi + αTi + Ti_5Si_3	
					1031; s	βTi + αTi + Ti_5Si_3 ↔ αTi + Ti_5Si_3	
			As-cast	1400	1081; w	βTi + Ti_5Si_3 ↔ βTi + αTi + Ti_5Si_3	
					1027 ± 5; s	βTi + αTi + Ti_5Si_3 ↔ αTi + Ti_5Si_3	

Table 6
Temperatures of invariant reactions in Ti—Al—Si compared to those in binary Ti—Al [39,43].

Reaction	Ti—Al—Si	Ti—Al [39,43]
$\beta Ti + \alpha Ti\ (+ Ti_5Si_3) \leftrightarrow Ti_3Al\ (+ Ti_5Si_3)$	1152 °C	1200 °C
$\alpha Ti\ (+ Ti_5Si_3) \leftrightarrow Ti_3Al + TiAl\ (+ Ti_5Si_3)$	1110 °C	1120 °C
$TiAl(1d\text{-}APS)\ (+ Ti_5Si_3) \leftrightarrow TiAl_2 + TiAl_3\ (+ Ti_5Si_3)$	1100 °C	977 °C
$\beta Ti + Ti_3Al\ (+ Ti_5Si_3) \leftrightarrow \alpha Ti\ (+ Ti_5Si_3)$	1095 °C	1170 °C

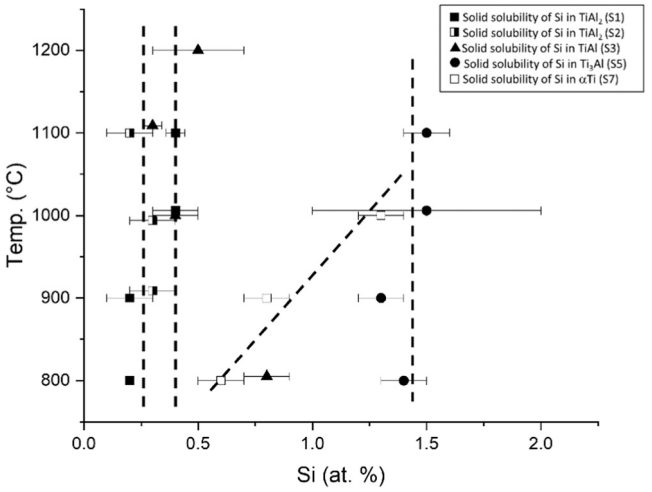

Fig. 12. The solid solubility of Si in αTi, Ti_3Al, TiAl, and $TiAl_2$ in dependence on temperature in alloys S7, S5, S3, S2 and S1 respectively.

determined for TiAl in alloys S2 and S4. From the shape of the single-phase field in Figs. 1, 3, 5, 8, 10 it is evident that 0.5 at% Si should also correspond to the maximum solid solubility of Si in TiAl. This value agrees with data measured for TiAl in as-cast alloys [16] and in a directionally solidified alloy [63], but is considerably lower than found in most previous studies, where 1–4 at% Si at 550 °C [32], 0.8 at% Si at 700 °C [30], 2–3 at% Si at 700 °C [28] and at 1000 °C [27], 1 at% Si at 1200 °C [17], and 1–1.5 at% Si in diffusion couples annealed between 700 and 1000 °C [26] were reported. On the other hand, no Si was detected by TEM-EDS in TiAl in a two-phase TiAl + Ti_5Si_3 alloy annealed at 1200 °C [59,64].

Data for S1 and S2 show that the solid solubility for Si in $TiAl_2$ is only about 0.3 at%, independent of temperature. This value is much smaller than any of those measured before, i.e. 1.4 at% Si at 550 °C [32], 1.5 at 700 °C [30], 1.8 at% Si at 900 °C [26], and 0.7 at% Si at 1000 °C [27]. $TiAl_3$ is the only binary Ti-Al phase with a marked solid solubility for Si, which exceeds 10 at% in equilibrium with $TiSi_2$ [15,17,25–27,30,62]. As no adequate alloy compositions have been studied, no additional information can be gained from the current investigation.

3.8. Solid solubility of Al in Ti_5Si_3

As detailed above, establishing the actual Al content of Ti_5Si_3 is difficult because it is not possible to equilibrate large, primary Ti_5Si_3 grains within reasonable annealing times. The established partial isothermal sections show that the maximum solid solubility for Al is always attained at the three-phase equilibrium Ti_5Si_3 + αTi or Ti_3Al + TiAl (Figs. 1, 3, 5, 8 & 10), which is observed in alloy S4. The data for S4 in Table 3 show a solid solubility of about 7 at% Al in Ti_5Si_3 at all investigated temperatures. Though there is some scatter in the data, the solid solubility for Al does only little, if at all, change with temperature. The maximum solid solubility of about 7 at% Al corresponds to the value reported by Manesh & Flower [47] for "fine silicides" extracted from the eutectic in an as-cast alloy. A similar value for the maximum solid solubility has also been reported in the 1200 °C isotherm by Schob et al. [17], however for the equilibrium βTi + Ti_3Al ("$Ti_{3-2}Al$") + Ti_5Si_3. Otherwise, mostly higher values have been measured, e.g., 10.9 at% Al for an alloy equilibrated at 1000 °C [27], 15–20 at% Al in samples prepared by self-propagating high-temperature synthesis (SHS) [35] or by ball milling [34,36]. However, for the latter case it has been shown that such high Al contents indicate metastable compositions of Ti_5Si_3 [36]. Higher solid solubilities of either 9.2 [64] or 13.4 at% Al [59] measured by TEM-EDS in Ti_5Si_3 after annealing for 12 h at 1200 °C are possibly due to a too short annealing time.

Significantly lower values for the maximum solid solubility of Al in Ti_5Si_3 were shown in the 1000 °C isotherm by Gupta [26] (3 at% Al) and in the 700 °C isotherm by Raman & Schubert [28] (5 at% Al). In both cases the maximum solid solubility is shown for phase equilibria with $TiAl_3$. According to the partial isothermal sections shown in Figs. 1, 3, 5, 8, 10, such low Al contents are reasonable for Ti_5Si_3 in equilibrium with $TiAl_3$, but do not correspond to the maximum solid solubility for Al, which is attained for Ti_5Si_3 + Ti_3Al + TiAl at these temperatures according to the present partial isothermal sections.

Zhang & Flower [65] showed that Al substantially increases the lattice constants of Ti_5Si_3, which was confirmed in [34,35], while

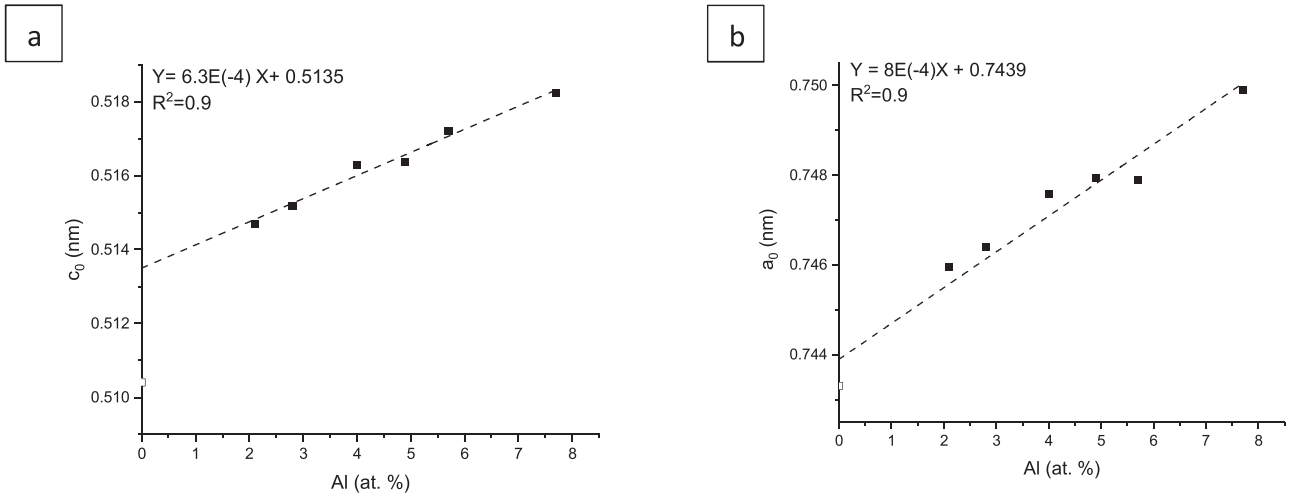

Fig. 13. a,b) Lattice constants of Ti_5Si_3 in relation to Al content; samples have been quenched from 1200 °C. Filled symbols are from current work, and open symbols are lattice constants of Ti_5Si_3 from binary Ti—Si [54].

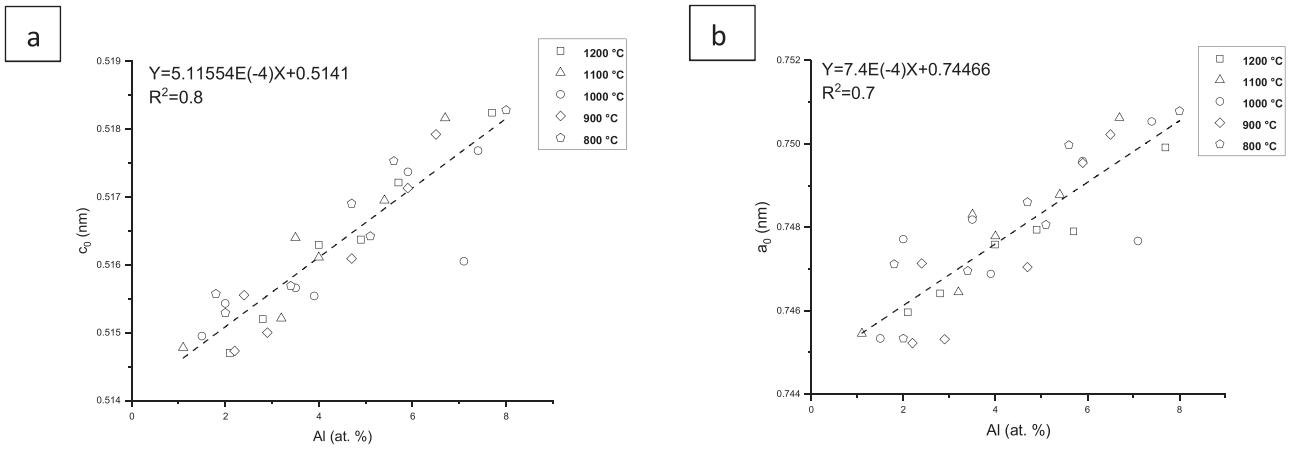

Fig. 14. a, b) Lattice constants of Ti_5Si_3 in relation to Al content; samples have been quenched from 800° to 1200°C.

according to Zha et al. [35] the addition of Al has almost no effect on the lattice constantss of Ti_5Si_3 and Bulanova et al. [16] showed a graph, where a_0 of Ti_5Si_3 first decreases, then increases and then decreases again with increasing Al content. To solve this conflicting evidence, lattice constants measured in samples annealed at 1200 °C are plotted in Fig. 13 and all lattice constants are shown in Fig. 14. Both figures show a steady increase of the lattice constants with increasing Al content. For samples annealed at 1200 °C the increase is even linear (Fig. 13), while for other temperatures there is more scatter of the data (Fig. 14). Comparing the data for different temperatures in Fig. 14**,** there is no evident dependence between annealing temperature and lattice constants. It is noted that, though lattice constants of Ti_5Si_3 show a strong dependence on Al content, they will also vary in dependence on Si content. However, data for Ti_5S_3 in S3 heat-treated at 1000 °C show the largest deviation in Fig. 14, which suggests that Ti_5Si_3 should actually have a lower Al content than the measured value in Table 3. A lower Al content would indeed fit much better to those Al contents measured for Ti_5Si_3 in S3 at all other temperatures.

The discrepancy in previous data is explained in that in [16,34,35] lattice constants were shown in dependence on the overall composition of the alloys and not on the actual Al content of Ti_5Si_3. The present results are therefore consistent with results by Kasraee et al. [34], who observed an increase of the lattice constants in “stoichiometric alloys” when they contained up to 7.5 at% Al, while no further increase was observed for higher Al contents. All samples in Zha et al. [35] were actually located in the three-phase field $TiAl_3$ + Ti_5Si_3 + Ti_5Si_4. Therefore it can be expected that the composition of Ti_5Si_3 is the same in all samples, hence, the lattice constants do not change with increasing Al content. Lattice constants in Bulanova et al. [16] were taken from alloys annealed at about 1300 °C, in which Ti_5Si_3 is in equilibrium with different phases. It is presumably therefore that latice constants show a “sinus curve behaviour” in dependence on the Al content.

4. Conclusion

Knowledge of the precise solid solubilities of Al in Ti_5Si_3 and Si in the Ti—Al phases is a perquisite for tailoring the microstructures and thereby the mechanical properties of TiAl-based alloys. From SEM, EPMA, XRD, TEM and DTA investigations, five partial isothermal sections between 800 and 1200 °C have been established.

No ternary phase was found and Ti_3Si was not detected in any of the alloys. The solid solubilities of Al in Ti_5Si_3 and Si in TiAl, $TiAl_2$ and Ti_3Al do not change in dependence on temperature. Lattice constants of Ti_5Si_3 for all heat-treated samples were calculated and results show that both lattice constants increase with increasing Al content. The partial vertical section of Si 9 at% shows that all established data are consistent. These data can now be employed to set up the next generation of advanced CALPHAD databases for the development of TiAl-based alloys with improved properties.

Funding sources

This project has received funding from the Clean Sky 2 Joint Undertaking under the European Union’s Horizon 2020 research and innovation programme under grant agreement No 820647.

CRediT authorship contribution statement

Zahra Kahrobaee: Data curation, Investigation, Formal analysis, Writing – original draft, Visualization, **Martin Palm:** Conceptualization, Validation, Writing – review and editing, Supervision, Project administration and funding acquisition.

Data availability

No data was used for the research described in the article.

Declaration of Competing Interest

The authors declare that they have no known competing financial interests or personal relationships that could have appeared to influence the work reported in this paper.

Acknowledgment

The authors would like to thank Mr. D. Klapproth and Mr. M. Kulse for alloy production, Mr. D. Kurz for wet chemical analysis, Mrs. I. Wossack and Mr. B. Breitbach for their help with performing EPMA and XRD analyses, respectively.

References

[1] B. Bewlay, M. Weimer, T. Kelly, A. Suzuki, P. Subramanian, The science, technology, and implementation of TiAl alloys in commercial aircraft engines, MRS Online Proc. Libr. 1516 (2013) 49–58, https://doi.org/10.1557/opl.2013.44
[2] H. Clemens, S. Mayer, Design, processing, microstructure, properties, and applications of advanced intermetallic TiAl alloys, Adv. Eng. Mater. 15 (2013) 191–215.
[3] J. Dai, J. Zhu, C. Chen, F. Weng, High temperature oxidation behavior and research status of modifications on improving high temperature oxidation resistance of titanium alloys and titanium aluminides: a review, J. Alloy. Compd. 685 (2016) 784–798, https://doi.org/10.1016/j.jallcom.2016.06.212
[4] X. Weihao, Z. Liang, J. Huiren, Effects of Si on high temperature oxidation resistance of TiAl alloy, J. -Beijing Univ. Aeronaut. Astronaut. 32 (2006) 365.

[5] D. Vojtěch, M. Mort'aniková, P. Novák, Kinetic and thermodynamic aspects of high-temperature oxidation of selected Ti-based alloys, Defect and Diffusion Forum, Trans Tech Publ Ltd, 2007, pp. 123–128, https://doi.org/10.4028/www.scientific.net/DDF.263.123

[6] P. Novák, Příprava, vlastnosti a použití intermetalických sloučenin, Chem. Listy 106 (2012) 884–889.

[7] S. Tsuyama, S. Mitao, K.-N. Minakawa, Alloy modification of γ-base titanium aluminide for improved oxidation resistance, creep strength and fracture toughness, Mater. Sci. Eng.: A (1992) 451–456.

[8] T. Noda, M. Okabe, S. Isobe, M. Sayashi, Silicide precipitation strengthened TiAl, Mater. Sci. Eng.: A 192 (1995) 774–779, https://doi.org/10.1016/0921-5093(94)03313-7

[9] M. Cabibbo, A. Knaislová, P. Novák, F. Průša, C. Paoletti, Role of Si on lamellar formation and mechanical response of two SPS Ti–15Al–15Si and Ti–10Al–20Si intermetallic alloys, Intermetallics 131 (2021) 107099, https://doi.org/10.1016/j.intermet.2021.107099

[10] U.R. Kattner, The Calphad method and its role in material and process development, Tecnol. em Metal., Mater. e Min. 13 (2016) 3, https://doi.org/10.4322/2176-1523.1059

[11] P. Perrot, Al-Si-Ti Ternary Phase Diagram Evaluation, in: G. Effenberg (Ed.), MSI Eureka, Materials Science International Services GmbH (MSI), Stuttgart, 2004.

[12] P. Perrot, G. Ti-Al-Si, G. Petzow, Effenberg (Eds.), Ternary alloys. A comprehensive compendium of evaluated constitutional data and phase diagrams, VIII, VCH, Weinheim, Germany, 1993, pp. 283–290.

[13] V. Raghavan, Al-Si-Ti (aluminum-silicon-titanium), J. Phase Equilibria Diffus 30 (2009) 82–83, https://doi.org/10.1007/s11669-008-9435-4

[14] V. Raghavan, Al-Si-Ti (aluminum-silicon-titanium), J. Phase Equilibria Diffus. 26 (2005) 624–628, https://doi.org/10.1361/154770305×74520

[15] M. Bulanova, L. Tretyachenko, M. Golovkova, K. Meleshevich, Phase equilibria in the α-Ti-Al-Si region of the Ti-Si-Al system, J. Phase Equilibria Diffus. 25 (2004) 209–229, https://doi.org/10.1007/s11669-004-0110-0

[16] M. Bulanova, L. Tretyachenko, M. Golovkova, Phase equilibria in the Ti-rich corner of the Ti-Si-Al system, Z. Met. 88 (1997) 256–265.

[17] O. Schob, H. Nowotny, F. Benesovsky, The ternary systems (Titanium, Zirconium, Hafnium)-aluminum-silicon, planseeber, Pluvermet 10 (1962) 65–67.

[18] D.H. Turner, F.A. Crossley, (Technical Report), D.J. McPherson, W. Rostoker (Eds.), The Titanium-rich corner of the Ti-Al-Si system in studies of phase relationships and transformation processes of Titanium-alloy systems, Wright Air Development Center, 1954, pp. 52–66 (Technical Report).

[19] F. Crossley, D. Turner, Titanium-rich corner of the Ti-Al-Si system, Trans. Met. Soc. AIME 212 (1958) 60–63.

[20] J. Li, S. Hao, Study of $\alpha(\alpha_2)/\gamma$ phase equilibria in the Ti-Al-Si ternary system, Acta Metall. Sin. -ENGL 32 (1996) 1171–1176.

[21] J. Li, Y. Zong, S. Hao, Effects of alloy elements (C, B, Fe, Si) on the Ti-Al binary phase diagram, J. Mater. Sci. Technol. 15 (1999).

[22] C.R. d F. Azevedo, H.M. Flower, Microstructure and phase relationships in Ti–Al–Si system, Mater. Sci. Technol. 15 (1999) 869–877, https://doi.org/10.1179/026708399101506661

[23] C.R. d F. Azevedo, H.M. Flower, Calculated ternary diagram of Ti–Al–Si system, Mater. Sci. Technol. 16 (2000) 372–381, https://doi.org/10.1179/026708300101507956

[24] C.R. d F. Azevedo, H.M. Flower, Experimental and calculated Ti-rich corner of the Al-Si-Ti ternary phase diagram, Calphad 26 (2002) 353–373, https://doi.org/10.1016/S0364-5916(02)00050-0

[25] J. Viala, N. Peillon, F. Bosselet, J. Bouix, Phase equilibria at 1000C in the Al-C-Si-Ti quaternary system: an experimental approach, Mater. Sci. Eng.: A 229 (1997) 95–113.

[26] S.P. Gupta, Intermetallic compounds in diffusion couples of Ti with an Al-Si eutectic alloy, Mater. Charact. 49 (2003) 321–330, https://doi.org/10.1016/S1044-5803(02)00342-X

[27] S. Liu, F. Weitzer, J.C. Schuster, N. Krendelsberger, Y. Du, On the reaction scheme and liquidus surface in the ternary system Al–Si–Ti, Int. J. Mater. Res. 99 (2008) 705–711, https://doi.org/10.3139/146.101702

[28] A. Raman, K. Schubert, The constitution of some alloy series related to $TiAl_3$. II. Investigations in Some T-Al-Si and $T^{4\cdots6}$-In Systems, Z. Met. 56 (1965) 44–52.

[29] J. Gröbner, D. Mirković, R. Schmid-Fetzer, Thermodynamic aspects of grain refinement of Al–Si alloys using Ti and B, Mater. Sci. Eng.: A 395 (2005) 10–21, https://doi.org/10.1016/j.msea.2004.11.048

[30] Z. Li, C. Liao, Y. Liu, X. Wang, Y. Wu, M. Zhao, Z. Long, F. Yin, 700° C isothermal section of the Al-Ti-Si ternary phase diagram, J. Phase Equilibria Diffus. 35 (2014) 564–574, https://doi.org/10.1007/s11669-014-0325-7

[31] Y. Li, Q.-F. Gu, Q. Luo, Y. Pang, S.-L. Chen, K.-C. Chou, X.-L. Wang, Q. Li, Thermodynamic investigation on phase formation in the Al–Si rich region of Al–Si–Ti system, Mater. Des. 102 (2016) 78–90, https://doi.org/10.1016/j.matdes.2016.03.144

[32] J. Wang, Y. Liu, Y. Liu, C. Wu, X. Su, The isothermal section of the Al-Si-Ti ternary system at 550 °C, J. Phase Equilibria Diffus. 40 (2019) 810–819, https://doi.org/10.1007/s11669-019-00774-4

[33] K. Kamei, T. Ninomiya, S. Hayashi, The phase diagram of the Al-Si-Ti equilibrium system, Metall. Abstr. Light Met. Alloy. 3 (1968) 67–70.

[34] K. Kasraee, A. Tayebifard, E. Salahi, Effect of substitution of Si by Al on microstructure and synthesis behavior of Ti_5Si_3 based alloys fabricated by mechanically activated self-propagating high-temperature synthesis, Adv. Powder Technol. 25 (2014) 885–890, https://doi.org/10.1016/j.apt.2014.01.008

[35] M. Zha, H.Y. Wang, S.T. Li, S.L. Li, Q.L. Guan, Q.C. Jiang, Influence of Al addition on the products of self-propagating high-temperature synthesis of Al–Ti–Si system, Mater. Chem. Phys. 114 (2009) 709–715, https://doi.org/10.1016/j.matchemphys.2008.10.024

[36] Z. Guan, T. Pfullmann, M. Oehring, R. Bormann, Phase formation during ball milling and subsequent thermal decomposition of Ti–Al–Si powder blends, J. Alloy. Compd. 252 (1997) 245–251, https://doi.org/10.1016/S0925-8388(96)02720-X

[37] Thermo-Calc Software AB, Next Generation TiAl Alloys Advanced by New European Consortium, ⟨https://thermocalc.com/blog/next-generation-tial-alloys-advanced-by-new-european-consortium/⟩.

[38] B. Distl, G. Dehm, F. Stein, Effect of oxygen on high-temperature phase equilibria in ternary Ti-Al-Nb Alloys, Z. Anorg. Allg. Chem. 646 (2020) 1151–1156, https://doi.org/10.1002/zaac.202000098

[39] J.C. Schuster, M. Palm, Reassessment of the binary Aluminium-Titanium phase diagram, J. Phase Equilibria. Diffus. 27 (2006) 255–277, https://doi.org/10.1361/154770306×109809

[40] L.S. T'sai, T.R. Hogness, The diffusion of gases through fused quartz, J. Phys. Chem. 36 (2002) 2595–2600.

[41] R. Kainuma, M. Palm, G. Inden, Solid-phase equilibria in the Ti-rich part of the Ti-Al system, Intermetallics 2 (1994) 321–332, https://doi.org/10.1016/0966-9795(94)90018-3

[42] Powder Diffraction File PDF-2, release 2004, International Center for Diffraction Data, Newtown Square, PA, USA (2004).

[43] M. Palm, Al-Ti binary phase diagram evaluation, in: G. Effenberg (Ed.), in: MSI Eureka, Materials Science International services GmbH (MSI), Stuttgart, 2020.

[44] M. Fiore, F. Beneduce, C.R.D.F. Azevedo, Assessment of the Ti-rich corner of the Ti-Si phase diagram: the recent dispute about the eutectoid reaction, Mater. Res. 19 (2016) 942–953, https://doi.org/10.1590/1980-5373-MR-2016-0157

[45] H.L. Lukas, N. Lebrun, Al-Si binary phase diagram evaluation, in: G. Effenberg (Ed.), MSI Eureka, MSI, Materials Science International Services GmbH, Stuttgart, 2004.

[46] C. Colinet, J.-C. Tedenac, Structural stability of intermetallic phases in the Si-Ti system. Point defects and chemical potentials in $D8_8$-Si_3Ti_5 phase, Intermetallics 18 (2010) 1444–1454, https://doi.org/10.1016/j.intermet.2010.03.028

[47] S.H. Manesh, H.M. Flower, Liquidus projection of Ti-Al-Si ternary system in vicinity of γ alloys, Mater. Sci. Technol. 10 (1994) 674–680, https://doi.org/10.1179/mst.1994.10.8.674

[48] P. Villars, L.D. Calvert, Pearson's Handbook of Crystallographic Data, 2ed...,, ASM International,, 1997.

[49] M.J. Blackburn, The ordering transformation in titanium- aluminum alloys containing up to 25 at% aluminum Trans, Met. Soc. AIME 239 (1967) 1200–1208.

[50] J. Braun, M. Ellner, B. Predel, Experimental investigations of the structure and stability of the TiAl phase, Z. Met. 86 (1995) 870–876.

[51] E. Illeková, P. Švec, D. Janičkovič, Influence of the processing on the ordering process in the Al-Ti binary system with composition close to Al_3Ti, Journal of Physics: Conference Series, IOP Publishing Ltd, 2009, pp. 1–6, https://doi.org/10.1088/1742-6596/144/1/012111

[52] H. Mabuchi, T. Asai, Y. Nakayama, Aluminide coatings on TiAl compound, Scr. Metall. 23 (1989) 685–689.

[53] J. Braun, M. Ellner, Phase equilibria investigations on the aluminum-rich part of the binary system Ti-Al, Metall. Mater. Trans. A 32 (2001) 1037–1047.

[54] V.N. Svechnikov, Y.A. Kocherzhinsky, L.M. Yupko, O.G. Kulik, E.A. Shishkin, Phase diagram of the titanium-silicon system, Dokl. Akad. Nauk, SSSR, 1970, pp. 393–396.

[55] M.J. Blackburn, Some aspects of phase transformations in titanium alloys, Some aspects of phase transformations in titanium alloys, Boeing Scientific Research Labs., Seattle, 1970, pp. 633–643, https://doi.org/10.1016/B978-0-08-006564-9.50071-3

[56] A. Hellwig, G. Inden, M. Palm, The invariant reaction between α, α_2 and γ in the Ti-Al system, Scr. Mater. 27 (1992) 143–148, https://doi.org/10.1016/0956-716X(92)90103-L

[57] R. Miida, M. Kasahara, D. Watanabe, Long-period antiphase domain structures of Al-Ti alloys near composition Al_3Ti, Jpn. J. Appl. Phys. 19 (1980) L707–L710.

[58] L. Zhang, G. Qiu, J. Wu, A preliminary research on the mechanical properties of TiAl+ Ti_5Si_3 dual phase alloys, MRS Online Proc. Libr. (OPL) 364 (1995), https://doi.org/10.1557/PROC-364-499

[59] F.-S. Sun, S.-E. Kim, C.-X. Cao, Y.-T. Lee, M.-G. Yan, A study of Ti_5Si_3/γ interface in TiAl alloys, Scr. Mater. 45 (2001) 383–389, https://doi.org/10.1016/S1359-6462(01)01012-0

[60] T. Takemoto, I. Okamoto, Intermetallic compounds formed during brazing of titanium with aluminium filler metals, J. Mater. Sci. 23 (1988) 1301–1308, https://doi.org/10.1007/BF01154593

[61] Q. Luo, Q. Li, J.-Y. Zhang, S.-L. Chen, K.-C. Chou, Experimental investigation and thermodynamic calculation of the Al–Si–Ti system in Al-rich corner, J. Alloy. Compd. 602 (2014) 58–65, https://doi.org/10.1016/j.jallcom.2014.02.107

[62] J.S. Wu, P.A. Beaven, R. Wagner, The $Ti_3(Al, Si)$+$Ti_5(Si, Al)_3$ eutectic reaction in the Ti-Al-Si system, Scr. Metall. Mater. 24 (1990) 207–212, https://doi.org/10.1016/0956-716X(90)90593-6

[63] J. Fan, X. Li, Y. Su, J. Guo, H. Fu, The microstructure parameters and microhardness of directionally solidified Ti–43Al–3Si alloy, J. Alloy. Compd. 506 (2010) 593–599, https://doi.org/10.1016/j.jallcom.2010.07.122

[64] F.-S. Sun, F.S. Froes, Precipitation of Ti_5Si_3 phase in TiAl alloys, Mater. Sci. Eng.: A 328 (2002) 113–121, https://doi.org/10.1016/S0921-5093(01)01678-1

[65] Z. Zhang, H.M. Flower, Composition and lattice parameters of silicide and matrix in cast Ti–Si–Al–Zr alloys, Mater. Sci. Technol. 7 (1991) 812–817, https://doi.org/10.1179/mst.1991.7.9.812